spectral requirements of local authorities.

3.6 RAKE Receivers

As stated before we concentrate on the reduced complexity RAKE receivers, namely PRake and SRake. The PRake is simply implemented assuming that the arrival time of the first multipath component is known (although this is not critical). The subsequent fingers are then just positioned at multiples of the finger width (in this case the pulse width, assumed to be 1 ns).

The SRake proposed here requires some additional complexity in implementation. Firstly the energy output by the correlators in response to a pilot symbol is sampled at the RAKE resolution. Fingers are then positioned at maximum energy positions in descending order. When a limited number of fingers are available, the SRake may be advantageous as it would capture more of the available energy.

In contrast, the conventional SRake requires knowledge of the channel (or high accuracy channel estimation). After this estimation, such a system would position its fingers at the largest arrival paths, again in descending order. The requirement for perfect channel estimation may make such a system impractical in implementation.

3.7 RAKE Combining

If we consider a RAKE receiver with J fingers, we can obtain the well known expression for instantaneous signal to noise ratio (i-SNR) [17]:

$$\gamma_s = \rho \frac{E_s}{\sigma_s^2} \frac{(\sum_{j=1}^{J} a_j g_j)^2}{\sum_{j=1}^{J} g_j^2}, \tag{20}$$

where g_j represent the RAKE weights and depend on the combining techniques used. ρ is the normalized correlation of a single pulse. E_s is the symbol energy of the transmitted signal and E_s/σ_s^2 is therefore regarded as the SNR of the transmitted signal. a represents the magnitudes of the arrival paths. For a given finger which had v arrival paths of magnitude α within its duration (see Eq. (3)), $a_j^2 = \sum_{i=1}^{v} \alpha_i^2$. The well known maximum ratio combining method (MRC) [17] can be obtained through applying the Cauchy inequality:

$$\gamma_s = \left(\sum_{j=1}^{J} a_j g_j \right)^2 \leq \sum_{j=1}^{J} a_j^2 \sum_{j=1}^{J} g_j^2, \tag{21}$$

which is equal only when $g_j = a_j$. The i-SNR for MRC is therefore:

$$\gamma_{s,MRC} = \rho \frac{E_s}{\sigma_s^2} \sum_{j=1}^{J} a_j^2, \tag{22}$$

3.8 Pilot Symbols

3.8.1 Correlator Estimation

For detection in the system (Eq. (18)) the receiver requires knowledge of the noiseless outputs of the correlators (vector $\mathbf{c}$) given by (14). This can be achieved by the transmission of suitable pilot symbols at the beginning of the packet. Naturally these symbols are transmitted in a noisy environment therefore only an estimate $\hat{\mathbf{c}}$ can be obtained.

One of the best methods for estimating values, vectors and/or functions in a noisy environment is the Kalman filter [20]. In this case it involves the simple case of measuring a fixed vector in noisy measurements using a Kalman filter. We use the following filter equations for k-th measurement from k pilot symbols:

$$K_k = \frac{P_{k-1}}{P_{k-1} + R} \tag{23a}$$

$$\hat{\mathbf{c}}_\mathbf{k} = \hat{\mathbf{c}}_{\mathbf{k-1}} + K_k(\hat{\mathbf{c}}_\mathbf{k}^* - \hat{\mathbf{c}}_{\mathbf{k-1}}) \tag{23b}$$

$$P_k = (1 - K_k)P_{k-1} \tag{23c}$$

where K is the filter gain, P is the error covariance in the estimate (we assume an initial value of 1), R is the measurement variance (related to the noise variance and given an initial value of 0.5 so as to cover a wide range of SNR values). $\hat{\mathbf{c}}_\mathbf{k}^*$ represents the measurement (or output of the correlators) and $\hat{\mathbf{c}}_\mathbf{k}$ is the estimate in response to the k-th pilot symbol.

To find the optimum number of pilot symbols required we analyze the average relative square error:

$$RSE(\hat{\mathbf{c}}) = \frac{|\mathbf{c} - \hat{\mathbf{c}}|}{|\mathbf{c}|}. \tag{24}$$

Figure 6 shows the average relative square error for the estimated $\hat{\mathbf{c}}$ in the major RAKE finger at different values of SNR. As can be seen the greater the number of pilot symbols the better the estimate of $\mathbf{c}$ becomes as the RSE reduces. By selecting a required RSE at a certain noise level we can find the optimum number of pilot symbols for the system. for example at 5 dB noise and an RSE of 0.2 it can be see that 20 pilots are needed when 4 elementary Hadamard-Hermites,

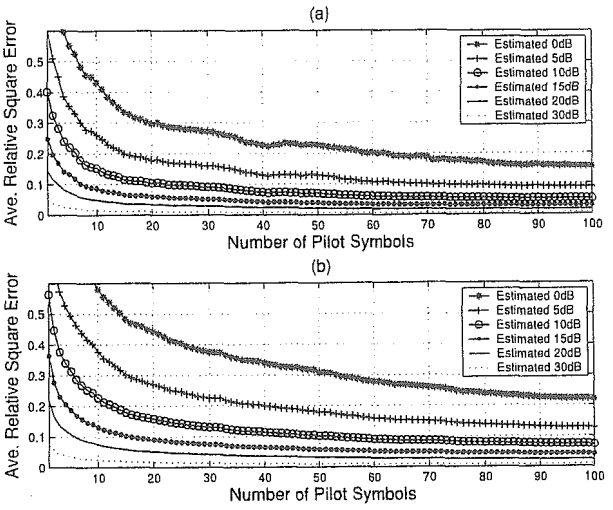

Fig. 6 Average relative square error versus number of pilot symbols k for RAKE fingers showing (a) 4 elementary Hadamard-Hermites and (b) 8 elementary Hadamard-Hermites.

and 50 pilots when 8 elementary Hadamard-Hermites are used.

3.8.2 Energy Scanning

Pilot symbols are also required for finding the position of fingers in the SRake structure. The energy output by the correlators is measured and sampled at the RAKE resolution to determine the best positions for the fingers of the SRake. Once again such pilots symbols are transmitted in a noisy environment. A small number of pilot symbols are required so as to satisfactorily position the SRake fingers. When multiple Pilot symbols are used, the energy measured at each sample time is simply averaged over the total number of pilots, and the positions of the RAKE fingers are determined.

4. Simulation Results

This section presents simulation results for a single user system. The pulse width is considered to be about 1 ns. The RAKE systems considered can only position the fingers at integer multiples of the pulse duration T (assumed to be 1 ns). A PRake system with j fingers therefore assumes that the arrival time of the first multipath component is known as the position of the first finger, and the subsequent fingers are then positioned at integer multiples of T thereafter. For the SRake system the best j positions in terms of maximum energy capture by the given set of correlators are used. The packet size is set to 1024 bits.

4.1 Number of Fingers

At first we assume that the system has perfect knowledge of the vector $\mathbf{c}$, and is also able to position the fingers of an SRake receiver ideally.

Figure 7 shows the comparison in bit error rate (BER) performance of the conventional single template system and the proposed system considering both PRake and SRake structures. The channel considered is the LOS CM1 channel. The plot shows the effect that increasing the number of fingers has on the performance of the system at fixed received E_b/N_0 levels.

It can clearly be seen that an increase in the number of fingers has the effect of improving the performance to an optimum point for all receivers considered. There is seen to be an optimum number of fingers to be used at any given noise level after which performance will degrade slightly. It is seen that in the CM1 channel, the optimum number of fingers (i.e. the number of fingers giving the best BER performance) is 15 for the PRake, and 10 for the SRake structure. Importantly it is also seen that the proposed RAKE finger structure outperforms the conventional system by a large margin. Significant gains in performance are achieved when using the proposed Hadamard-Hermite space.

It was noted that there is an optimum number of fingers in the system. Increasing the number of fingers above

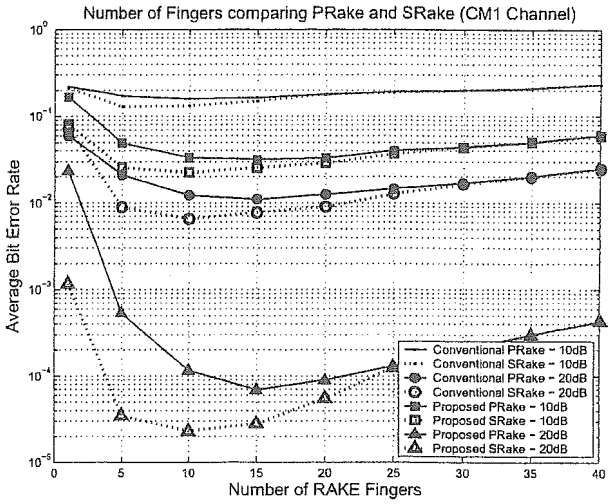

Fig. 7 Average bit error rate performance comparing PRake and SRake receivers on CM1 with increasing numbers of RAKE fingers at fixed E_b/N_0 levels as indicated. Conventional and proposed systems using 8 elementary shapes are shown.

this optimum number actually shows a slight performance degradation. The reason is that most of the significant multipath components that arrive at the receiver in the CM1 channel occur in the first 25 ns. Thereafter the components which arrive have much lower energy. Decisions in these low energy fingers will start to be affected by the significant noise compared to the signals that are received in those components. Decoding decisions relying on these low power components actually has a deterioration effect on the BER as can be seen.

Another important conclusion that can be drawn from this plot is that for a given number of RAKE fingers the SRake system will have a slightly better performance than the PRake, especially when the number of fingers is low. Effectively, the SRake requires fewer fingers to achieve a certain BER than the PRake does. In the LOS channel the major paths arrive very close to the beginning of the multipath spread so the performance of the two types of receivers will converge with larger numbers of fingers.

Figure 8 now considers the same PRake and SRake structures on the NLOS channel CM2. Due to the absence of a direct LOS component and a denser multipath environment, it is seen that the PRake has a much more linear performance than observed in Fig. 7 and requires more fingers to reach a required performance level. Once again it is clear from the plot that the proposed system offers a significant improvement over the conventional RAKE receivers. The optimum numbers of fingers are now seen to be 25 for the PRake structure and 15 for the SRake structure.

It is observed that the performance of the PRake in this CM2 channel is poorer than before with a small number of fingers. This is due to the initial arrival paths having less energy than those in CM1. It is noted that the arrival paths are not necessarily concentrated at the beginning of the multipath spread in this NLOS situation. This can be attributed to

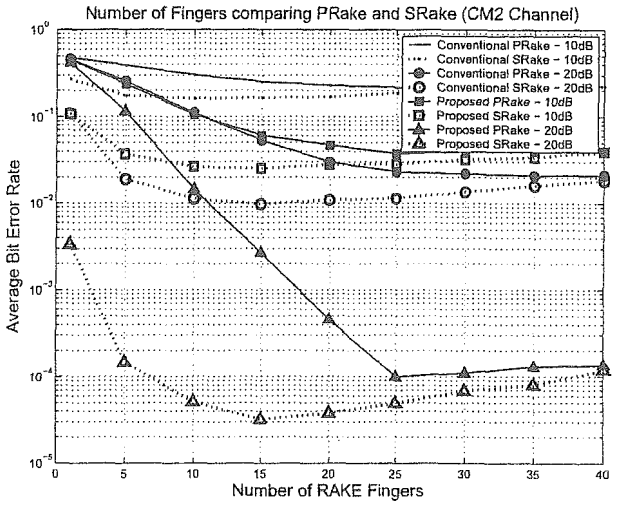

Fig. 8 Average BER comparing PRake (solid lines) and SRake (dotted lines) receivers on CM2 with increasing RAKE fingers at different received E_b/N_0 levels.

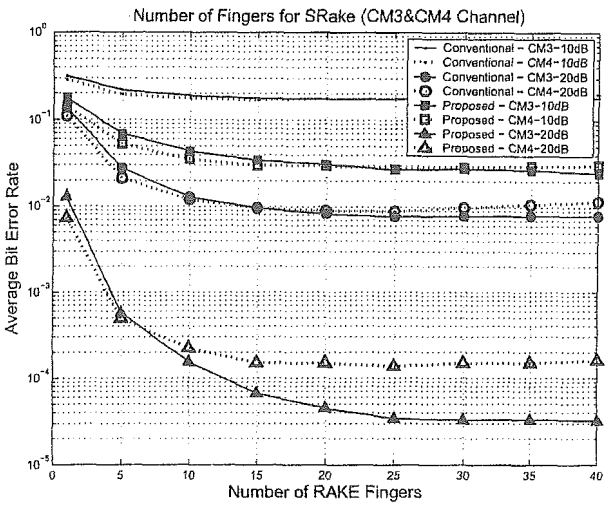

Fig. 9 Average BER comparing SRake receivers on CM3 and CM4 with increasing RAKE fingers at different received E_b/N_0 levels.

the fact that the most significant paths are also not necessarily positioned near to the first arrival path. A larger number of paths with an increased delay spread means that far more fingers are required in the PRake system to achieve a certain level of performance as more energy needs to be effectively captured. Due to the fact that the finger resolution is 1 ns in these simulations, the proposed system is capable of effectively utilizing more of the received energy when more paths are available in each finger than the conventional RAKE receivers. The SRake is seen to have a large improvement in performance over the PRake in this channel situation. A significantly lower number of fingers are required to achieve the same, and often a better, error performance when using the SRake. The added complexity of the SRake structure may be considered advantageous due to the significant reduction in the number of fingers required to meet a certain BER performance.

Figure 9 shows the results obtained for conventional and proposed SRake receivers on the CM3 and CM4 channel models. Due to the increased delay spread in the channel, the PRake structure was found to be ineffective and results are not shown here. To obtain useful results using such a PRake structure on these channels (CM3 and CM4), impractical numbers of fingers are required. The PRake using less fingers would not capture sufficient useful energy for successful symbol detection. The advantages of the proposed system over the conventional system employing SRake structure can again clearly be observed as vast improvements in the error performance are obtained. The optimum number of fingers is seen to be about 25 on both CM3 and CM4. The error performance hereafter flattens out and shows only a slight decrease in performance as the number of fingers increases. This is due to the increased delay spread of the channel, meaning that more of the 40 fingers shown will contain energy that is significant or at least comparable to noise. If many more fingers were considered a decrease in error performance would again be observed.

This subsection shows that the proposed Hadamard-Hermite decomposition Rake Receiver has better performance in all 4 channel models proposed by the IEEE. The more realistic situation needs to be considered where perfect knowledge of the correlator outputs or energy along the delay spread is not known. As has been mentioned pilot symbols are used at the beginning of each packet for this purpose. As stated 50 pilot symbols are used for estimating the vector $\mathbf{c}$, and an additional 20 are used to accurately measure energy and position the fingers of the SRake. The reduction in performance due to this pilot estimation will be observed in the full BER simulations that follow.

4.2 BER

We now consider the overall Bit Error Rate (BER) performance of the system. We further analyze the situation in terms of the full received E_b/N_0. E_b is defined as the expected received energy per information bit that takes the IEEE channel model normalization into consideration as well as the loss due to using pilot symbols,

$$Loss = 10\log_{10}\frac{N_b}{N_b + N_{Pc} + N_{PE}}, \tag{25}$$

where N_b is the number if information bits, N_{Pc} is the number of pilot symbols used to estimate $\mathbf{c}$ and N_{PE} is the number of pilot symbols used to position the fingers in the SRake structure. Performance degradation due to inaccuracies in the estimate of $\mathbf{c}$ as well as in poor positioning of the fingers will occur.

Figure 10 shows a plot of the BER for PRake and SRake structures utilizing the optimum number of fingers on the LOS CM1 channel. As can be clearly seen the proposed RAKE finger structure shows vast performance improvements for both PRake and SRake receivers over their conventional counterparts. In addition it is also evident that

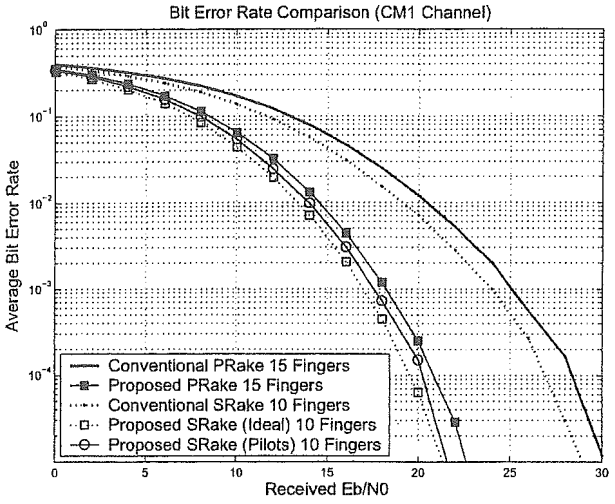

Fig. 10 Average BER PRake and SRake receivers on CM1.

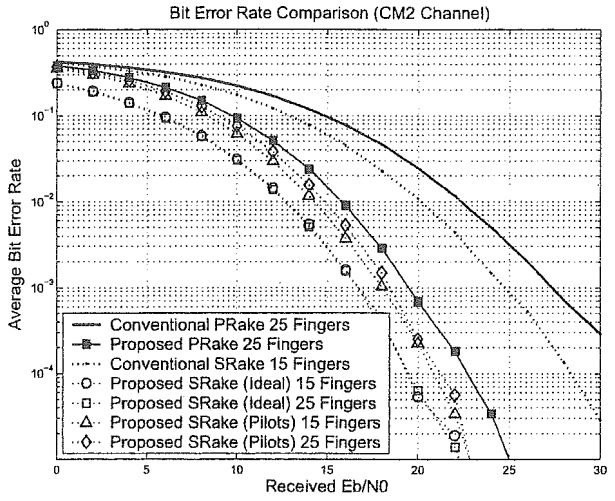

Fig. 11 Average BER PRake and SRake receivers on CM2.

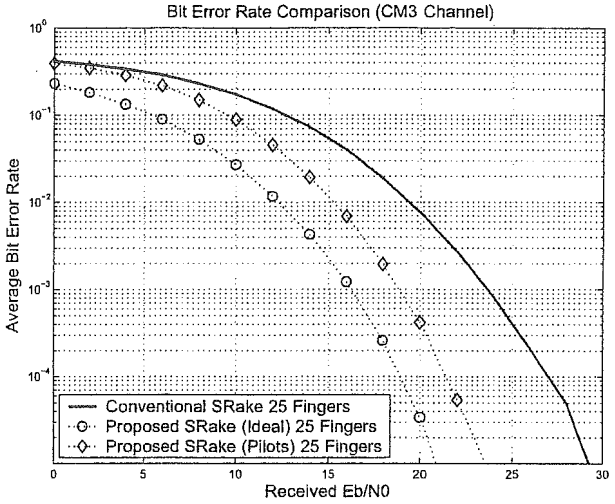

Fig. 12 Average BER PRake and SRake receivers on CM3 with varying numbers of fingers.

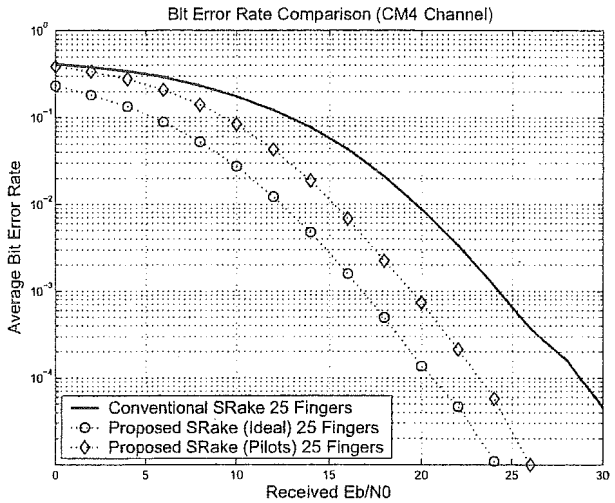

Fig. 13 Average BER PRake and SRake receivers on CM4 with varying numbers of fingers.

the difference in performance between the SRake and PRake receivers are relatively small. This is again due to the fact that most of the energy is contained within the first few tens of nanoseconds in the LOS CM1 channel and is in line with the previous observations. In addition plots for the proposed SRake structure showing the ideal situation, where perfect knowledge of $\mathbf{c}$ and perfect finger positioning is available (marked (Ideal)), as well as the situation where pilot symbols are used to estimate $\mathbf{c}$ and finger positions (marked (Pilots)) are shown. It is clear that there is a small reduction in performance is caused by this addition of pilots.

Figure 11 compares the BER performance of the conventional and proposed receivers in the NLOS channel CM2. Once again the significant performance improvements with the proposed structure over the conventional structure can be seen. Improvement of more than 5 dB is seen at many BER levels for both PRake and SRake structures. It is however again noticed that there is a slight reduction in performance when comparing the SRake (Ideal) with perfect knowledge of $\mathbf{c}$ and perfect finger positioning to the SRake (Pilots) which has to estimate these values. With 25 fingers in CM2 it is seen that the SRake structure employing pilot symbols shows about a 2 dB performance advantage over the PRake structure. The performance improvement obtained using the SRake structure may be seen as being advantageous in this situation. Plots of the proposed SRake employing only the optimum 15 fingers are also included, and illustrate an even better performance over the SRake with 25 fingers can be achieved. Importantly this SRake with 15 fingers also out preforms the PRake with 25 fingers. This further emphasizes the advantage of the SRake structure in the NLOS channel. The cause of this insignificant loss of performance is that the vast majority of the energy in the multipath is contained in a small number of major com-

ponents (15 in this case), which are selected with priority by the SRake. Selecting further fingers would only degrade the performance as was seen in the previous subsection. Further improvements can be obtained if coding and repetition were employed.

Figures 12 and 13 show the results when the system is applied on the CM3 and CM4 channel models. The proposed SRake structure is again seen to vastly outperform the conventional system. The interpulse interference in the conventional system leads to the major performance degradation observed in the conventional system. Similar performance gains are therefore observed in all 4 channel models proposed by the IEEE.

5. Conclusions

In conclusion this paper represented a novel finger-wise modification to the standard RAKE receiver. By using a Hadamard-Hermite subspace the proposed system showed significantly better performance than the conventional approach in simulation results. The effects of intrapulse interference due to the finger spacing being much larger than the typical multipath resolution can be reduced using this approach. Far fewer RAKE fingers would be required to obtain similar levels of performance than in the conventional system. Fewer RAKE fingers in the system may make it more practical to implement in reality.

It is also noted that the approach used here is largely independent of the order of the Hermite. A similar procedure to that considered here could be followed for different pulse shapes. In addition it should be noted that this approach may also be useful in combatting any other distortions that remain constant for the duration of the packet. This implies that any antenna distortion may also be compensated for in a similar fashion. The performance, under these circumstances needs to be investigated. In future we intend to analyze this as well as well as the possibilities of implementing different modulation schemes.

References

[1] M.Z. Win and R.A. Scholtz, "Impulse radio: How it works," IEEE Commun. Lett., vol.2, no.2, pp.36–38, Feb. 1998.

[2] M.Z. Win and R.A. Scholtz, "Ultra-wide bandwidth time-hopping spread-spectrum impulse radio for wireless multiple-access communications," IEEE Trans. Commun., vol.48, no.4, pp.679–691, April 2000.

[3] J. Foerster, "Channel modeling sub-comittee report final," IEEE P802.15 Working Group for Wireless Personal Area Networks (WPANs), IEEE P802.15-02/490r1-SG3a, Feb. 2003.

[4] M.Z. Win and R.A. Scholtz, "Characterization of ultra-wide bandwidth wireless indoor channels: A communication-theoretic view," IEEE J. Sel. Areas Commun., vol.20, no.9, pp.1613–1627, Dec. 2002.

[5] A. Álvarez, G. Valera, M. Lobeira, R. Torres, and J.L. García, "Ultrawideband channel characterization and modelling," Proc. IEEE 1st International Workshop of UWB Systems (IWUWBS'03), Oulu, Finland, June 2003.

[6] J. Keignart and N. Daniele, "Channel sounding and modelling for indoor uwb communications," Proc. IEEE 1st International Workshop of UWB Systems (IWUWBS'03), Oulu, Finland, June 2003.

[7] M. Win, G. Chriskos, and N.R. Sollenberger, "Performance of Rake reception in dense multipath channels: Implications of spreading bandwidth and selection diversity order," IEEE J. Sel. Areas Commun., vol.18, no.2, pp.1516–1525, Aug. 2000.

[8] B. Mielczarek, M. Wessman, and A. Svensson, "Performance of coherent UWB rake receivers with channel estimators," Vehicular Technology Conference 2003, VTC 2003-Fall, vol.3, pp.1880–1884, Oct. 2003.

[9] S. Franz and U. Mitra, "Integration interval optimization and performance analysis for UWB transmitted reference systems," Proc. IEEE Joint UWBST and IWUWBS04, pp.26–30, Kyoto, Japan, May 2004.

[10] J. Romme and G. Durisi, "Transmit reference impulse radio systems using weighted correlation," Proc. IEEE Joint UWBST and IWUWBS04, pp.141–145, Kyoto, Japan, May 2004.

[11] C.J. Mitchell, G. Abreu, and R. Kohno, "Combined pulse shape and pulse position modulation for high data rate transmissions in UWB communications," Int. J. Wirel. Inf. Netw., vol.4, no.10, pp.167–178, Oct. 2003.

[12] G. Abreu, C.J. Mitchell, and R. Kohno, "On the design of orthogonal pulse-shape modulation for UWB systems using Hermite pulses," J. Commun. Netw., vol.5, no.4, pp.328–343, Dec. 2003.

[13] M. Ghavami, L.B. Michael, and R. Kohno, "Hermite function based orthogonal pulses for ultra wideband communications," Proc. WPMC'01, pp.437–440, Aalborg, Denmark, 2001.

[14] A. Saleh and R. Valenzuela, "A statistical model for indoor multipath paropagation," IEEE J. Sel. Areas Commun., vol.SAC-5, no.2, pp.128–137, Feb. 1987.

[15] D. Cassioli, M. Win, F. Vatalaro, and A.F Molisch, "Effects of spreading bandwidth on the performance of UWB Rake receivers," Mitsubishi Research Laboratory Report, TR-3003065, Aug. 2003.

[16] M. Win and Z.A. Kostic, "Virtual path analysis of selective Rake receiver in dense multipath channels," IEEE Commun. Lett., vol.3, no.11, pp.308–310, Nov. 1999.

[17] J. Zhang, R.A. Kennedy, and T.D. Abhayapala, "Conditions and performance of ideal RAKE reception for ultra-wideband signals in lognormal fading channels," Int. J. Wirel. Inf. Netw., vol.4, no.10, pp.193–200, Oct. 2003.

[18] J.G. Proakis, Digital Communications, Fourth ed., McGraw-Hill, New York, 2000.

[19] A. Armogida, B. Allen, M. Ghavami, M. Porretta, G. Manara, and H. Aghvami, "Path loss modelling in short range UWB transmissions," Proc. IEEE 1st International Workshop of UWB Systems (IWUWBS'03), Oulu, Finland, June 2003.

[20] G. Welch and G. Bishop, "An introduction to the Kalman filter." University of North Carolina-Chapel Hill, TR 95-041, April 2004.

[21] A.D. Poularikas, The Transforms and Applications Handbook, 2nd ed., CRC Press, Boca Raton, FL, 2000.

Craig John Mitchell was born in Johannesburg, South Africa in November 1975. He received both his B.Sc. (*summa cum laude*) and M.Sc. in electrical engineering from the University of the Witwatersrand, South Africa in 1997 and 2001, respectively. He is currently working towards his Ph.D. at the Yokohama National University, Japan. His research interests lie in the areas of ultra-wideband systems, coding and wireless communications. He was the recipient of the Uenohara Foreign Student's Award for Excellence in Research in 2004.

Giuseppe Abreu was born in Salvador-Bahia, Brazil in December 1972. He received his B.E. in electronics engineering from the Federal University of Bahia, Brazil, in 1996. From April 1997 to March 2004, he was a research with the Kohno Laboratory of the Yokohama National University, Japan, where he obtained his M.E. and Ph.D. degrees in electrical and computer engineering. He was also the recipient of the Uenohara Foreign Student's Award for Excellence in Research from the University of Tokyo in 2000. He has authored and co-authored 2 internationally registered patents (for Sony Corporation, Japan), a few international journal papers and various conference papers. He is currently with the Center for Wireless Communications at the University of Oulu, Finland. His current research interests include Smart Antennas, Beampattern Synthesis, Space-Time Signal Processing and Coding, MIMO Systems and Ultra Wideband Communications.

Ryuji Kohno received the Ph.D. degree from the University of Tokyo in 1984. Dr. Kohno is currently a Professor of the Division of Physics, Electrical and Computer Engineering, Yokohama National University. In his career he was a director of Advanced Telecommunications Laboratory of SONY CSL during 1998–2002 and currently a director of UWB Technology institute of National Institute of Information and Communications Technology (NICT). In his academic activities, he was elected as a member of the Board of Governors of IEEE Information Theory (IT) Society in 2000 and 2003. He has played a role of an editor of the IEEE Transactions on IT, Communications, and Intelligent Transport Systems (ITS). He is a vice-president of Engineering Sciences Society of IEICE and has been the Chairman of the IEICE Technical Committee on Spread Spectrum Technology, that on ITS, and that on Software Defined Radio (SDR). Prof. Kohno has contributed for organizing many international conferences, such as a chair-in honor of 2002 & 2003 International Conference of SDR (SDR'02 & SDR'03), a TPC co-chair of 2003 International Workshop on UWB Systems (IWUWBS'03), and a general co-chair of 2003 IEEE International Symposium on IT (ISIT'03), that of Joint UWBST&IWUWB'04 and so on. He was awarded IEICE Greatest Contribution Award and NTT DoCoMo Mobile Science Award in 1999 and 2002, respectively.

Low-Complexity Bit-Interleaved Coded DAPSK for Rayleigh-Fading Channels

Koji Ishibashi, *Student Member, IEEE*, Hideki Ochiai, *Member, IEEE*, and Ryuji Kohno, *Member, IEEE*

***Abstract*—We analyze the achievable performance of bit-interleaved coded differential amplitude and phase-shift keying (DAPSK) systems over frequency nonselective Rayleigh-fading channels with suboptimal differential detection assuming an ideal bit interleaving. The suboptimal differential detection in this work refers to the bit metric calculation based only on the *difference* between two consecutive symbols, in contrast to more complex maximum-likelihood (ML)-based differential detection, which makes use of all the observed consecutive symbols for its metric calculation in channel decoding. As benchmarks of coded system performance, we analyze the average mutual information (AMI) and cutoff rate of this system. Exact probability density functions of the suboptimal differential detector outputs are derived for this purpose. Comparative studies suggest that the performance loss of the suboptimal approach is in fact noticeable. Therefore, we also develop a low-complexity receiver structure in the framework of suboptimal differential detection that can approach the performance of ML-based system by suitably incorporating the amplitude statistics of received symbols. The theoretical framework developed in this paper is also confirmed by simulations using convolutional and turbo codes.**

***Index Terms*—Average mutual information (AMI), bit-interleaved coded modulation (BICM), cutoff rate, differential amplitude and phase-shift keying (DAPSK), differential detection, metric calculation, receiver complexity.**

I. Introduction

OVER THE YEARS, differential detection has been a preferable choice for mobile communications systems due to its robustness against phase ambiguities induced by rapid fading. Combined with orthogonal frequency-division multiplexing (OFDM), it can also cope with frequency-selective channels even without accurate channel estimation, thus resulting in a simple receiver structure [1].

Differential detection in its original form literally makes use of only the *difference* between two consecutive received symbols. Although this type of differential detection enjoys very low-complexity and robustness against fading channels, its well-known drawback is the performance loss relative to coherent detection over static and stationary channels, where an accurate reference symbol can readily be estimated. In contrast, more recent techniques, such as *multiple symbol differential detection* (MSDD) [2]–[5], can reduce this gap by observing several consecutive differentially encoded symbols based on maximum-likelihood (ML) criterion. The major drawback of MSDD is its complexity, which grows exponentially with the observation symbol interval. Therefore, various computational reduction techniques have been proposed in the literature to mitigate this prohibitive computational overhead (see, e.g., [6]–[12]).

In order to achieve high bandwidth efficiency with high reliability, the use of coded modulation and, thus, an expansion of constellation size is necessary. One approach that can achieve this without loss of differential detectability is the use of differential amplitude and phase shift keying (DAPSK) [1], [13], in conjunction with coded modulation. One of the important design criteria in this scenario is the calculation of the bit metric required for the subsequent channel decoder. Recently, in [9] and [14], the performance of DAPSK with coded modulation has been analyzed, where the metric in conjunction with MSDD has been employed, with a main focus on the performance difference between the two types of coded modulation, namely, bit-interleaved coded modulation (BICM) [15], [16] and multilevel coding (MLC) [17], [18].

In general, the use of MSDD metric for DAPSK is computationally demanding. Furthermore, even with the conventional two-symbol observation case, the metric calculation based on the ML criterion becomes a limiting factor if the constellation size is large, as the complexity grows exponentially with the number of bits in the signal constellation. An alternative suboptimal approach is to calculate the metrics of amplitude and phase separately. Specifically, from two consecutive received symbols, one may extract envelope and phase differences separately, each used for calculation of the corresponding bit metrics. This work is focused on this separate demodulation and decoding approach to achieve low complexity.

The question that may arise at this point is how much the performance loss of this suboptimal decoding is, compared with the ML-based decoding under the same two-symbol observation constraint. Therefore, in this paper, we quantitatively analyze the performance of suboptimal approaches in terms of average mutual information (AMI) and cutoff rate. For simplicity, we consider the scenario of BICM and Rayleigh fading with ideal bit interleaving throughout this paper. The exact formulas of the associated probability density functions (pdfs) are derived for this purpose. It turns out that compared with the ML-based metric calculation with the two-symbol observation, which we shall refer to as maximum-likelihood differential detection (MLDD) for simplicity, the loss caused by the suboptimal approach is in fact noticeable. Therefore, we further develop simple bit metrics that can approach the performance of MLDD, while retaining low complexity. In [19], a suboptimal

Manuscript received March 31, 2004; revised February 6, 2005 and February 28, 2005. This paper was presented in part at the IEEE International Conference on Communications (ICC 2004), Paris, France, June 2004.

The authors are with the Division of Physics, Electrical and Computer Engineering, Yokohama National University, Yokohama 240-8501, Japan (e-mail: koji@ieee.org).

Digital Object Identifier 10.1109/JSAC.2005.853879

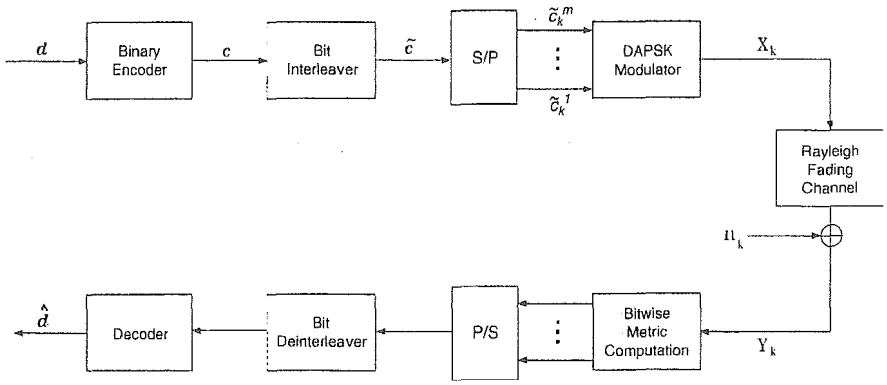

Fig. 1. System model of bit-interleaved coded DAPSK over Rayleigh-fading channels.

metric for DAPSK in conjunction with BICM has been proposed based on the Gaussian approximation of the associated pdfs. It will be shown by computer simulation that our proposed metric derived from the exact pdfs outperforms that of [19] in a high signal-to-noise ratio (SNR) regime.

In the literature, the cutoff rate of differential phase-shift keying (DPSK) system over an additive white Gaussian noise (AWGN) channel is discussed in [20] and [21], and the channel capacity is studied in [22] and [23], all associated with MSDD. The AMI and cutoff rate of conventional two-symbol DPSK over fading channels with and without the knowledge of amplitude have been studied in [24]. The performance of uncoded DAPSK has been extensively studied in the literature (see, e.g., [25]), and the AMI associated with MSDD is calculated in [9] and [14]. However, the exact analysis of AMI and cutoff rate for the suboptimal cases discussed above appears to be new.

This paper is organized as follows. Section II describes the system model considered throughout this paper, Section III is devoted to the analysis of BICM-DAPSK with the suboptimal approach in terms of AMI and cutoff rate. In Section IV, we propose improved bit metrics for the Viterbi and iterative *a posteriori*probability (APP) decoders. In order to justify our theoretical framework, computer simulations are performed with the proposed bit metrics in Section V. Finally, concluding remarks are given in Section VI.

II. System Model of Bit-Interleaved Coded DAPSK

A. Transmitter Model

The overall system model is illustrated in Fig. 1. At the transmitter, a binary information sequence $\boldsymbol{d}$ is encoded by a binary channel encoder. The resulting binary code word of length N, $\boldsymbol{c} = [c_0, c_1, \cdots, c_{N-1}] \in \{0,1\}^N$, is followed by the bit interleaver, which generates the bitwise interleaved sequence $\tilde{\boldsymbol{c}}$. Let $\mathcal{X}$ denote a set of complex signal points with $|\mathcal{X}| = 2^m$. Each m-tuple of the bit interleaver outputs at time instant k, $\tilde{\boldsymbol{c}}_k = [\tilde{c}_k^1, \tilde{c}_k^2, \ldots, \tilde{c}_k^m]$, is then mapped to $X_k \in \mathcal{X}$ (note that $k = 0, 1, \cdots, N/m$ and we assume that $k = 0$ corresponds to the initial reference symbol index). Since we apply differential encoding, the mapping should also depend on the previous symbol X_{k-1}.

DAPSK, also known as a star quadrature amplitude modulation (QAM) [13], is a combination of 2^n-DASK and 2^{m-n}-DPSK constellations. The signal constellation set $\mathcal{X}$ of DAPSK is composed of 2^n concentric circles of 2^{m-n}-PSK, each circle having a radius of α^i, with $i = 0, 1, \ldots, 2^n - 1$. The parameter α is referred to as a *ring ratio* and its typical value is 2.0 for 16-DAPSK [26].

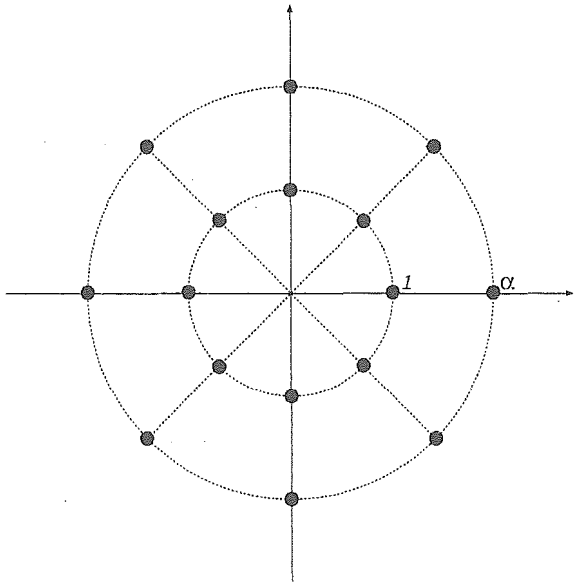

Fig. 2. Complex signal constellation of 16-DAPSK: $\alpha = 2.0$ is adopted with the inner ring normalized to unity.

Throughout this paper, we consider the case of $m = 4, n = 1$, and $\alpha = 2.0$ for simplicity. In this case, the signal constellation is the 16-DAPSK shown in Fig. 2. Let a_k and ψ_k denote the amplitude and phase of X_k, respectively. The first n bits of $\tilde{\boldsymbol{c}}_k$, $[\tilde{c}_k^1, \tilde{c}_k^2, \ldots, \tilde{c}_k^n]$, choose the amplitude difference between two successive symbols a_{k-1} and a_k. For the 16-DAPSK system above, the coded bit $\tilde{c}_k^1 \in \{0,1\}$ chooses $a_k \in \{1, \alpha\}$ by the following rule:

$$a_k = \begin{cases} a_{k-1}, & \text{for } \tilde{c}_k^1 = 0 \\ \bar{a}_{k-1}, & \text{for } \tilde{c}_k^1 = 1 \end{cases} \tag{1}$$

where $\bar{a}$ denotes flipping of the state of a ($\bar{a} = 1$ or α for $a = \alpha$ or 1, respectively). For the DPSK part, the remaining $(m - n)$ bits of $\tilde{\boldsymbol{c}}_k$, $[\tilde{c}_k^{n+1}, \tilde{c}_k^{n+2}, \ldots, \tilde{c}_k^m]$, choose the phase difference $\Delta\psi_k = \psi_k - \psi_{k-1}$ with Gray labeling [15].

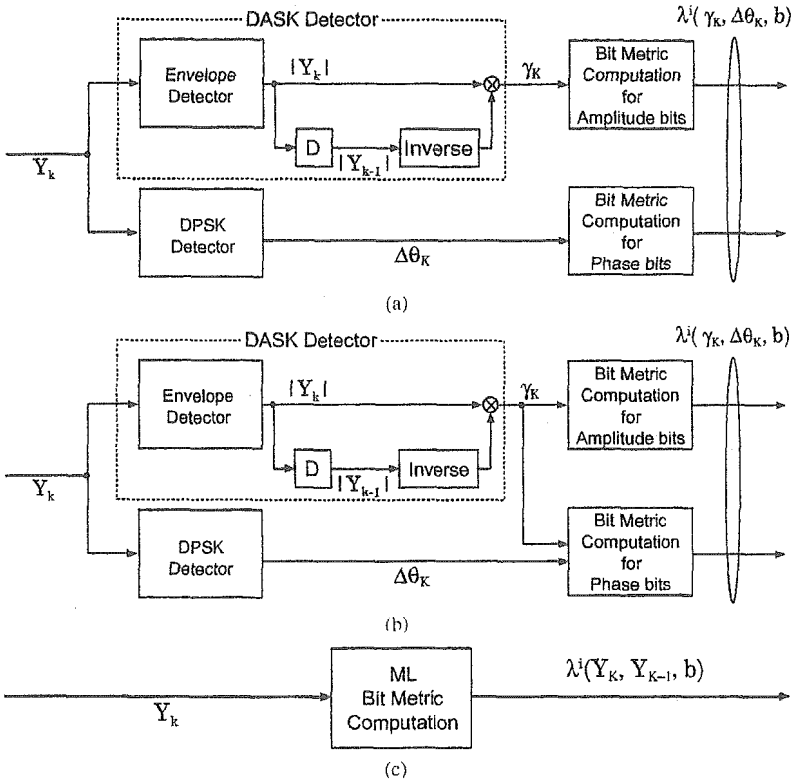

Fig. 3. Block diagrams of three receiver structures. (a) Separate differential detection. (b) Partially combined differential detection. (c) ML differential detection.

B. Channel Description

Throughout this paper, the channel is assumed to be frequency nonselective Rayleigh fading. The channel output Y_k corresponding to an input X_k can be expressed as

$$Y_k = \rho_k e^{j\phi_k} X_k + n_k \tag{2}$$

where n_k is the complex AWGN with zero mean and variance $2\sigma^2$ per complex dimension, sampled at time instant k. The amplitude ρ_k and phase ϕ_k of the fading coefficient, thus, follow Rayleigh and uniform distributions, respectively.

In order to make theoretical analysis tractable, the following assumptions are made. First, the fading process is wide-sense stationary and slow enough to be time-invariant at least during the two consecutive symbol intervals. Hence, it follows that $\rho_k = \rho_{k-1}$ and $\phi_k = \phi_{k-1}$ for any k. Second, the bit interleaving is ideal such that it fully eliminates the fading correlations of consecutive bits after bitwise deinterleaving at the receiver, i.e., the channel is *memoryless*.

These assumptions commonly appear in the literature of coded modulation systems with noncoherent detection (e.g., [9] and [27]–[29]).

C. Suboptimal Differential Detections

The simplest differential detection scenario for the coded DAPSK system consists of two separate detectors, each detecting envelope and phase differences [see Fig. 3(a)]. To detect the envelope difference, the amplitude ratio γ_k is calculated by $\gamma_k = |Y_k|/|Y_{k-1}|$, where $|Y_k|$ denotes the envelope of kth output symbol. Likewise, the phase difference is calculated by $\Delta\theta_k = \theta_k - \theta_{k-1}$, where $\theta_k = \angle Y_k$ and $\Delta\theta_k \in [-\pi, \pi)$. In this scenario, γ_k and $\Delta\theta_k$ are separately used to compute the associated bit metrics for amplitude and phase, respectively. Thus, γ_k and $\Delta\theta_k$ are assumed to be mutually statistically independent random variables. This approach, illustrated in Fig. 3(a), will be called a *separate differential detection* (SDD) in the following.

Let $\lambda^i(\gamma_k, \Delta\theta_k, b)$ denote a bit metric associated with the decision that the ith bit of the kth symbol is equal to b, where $i = 1, \ldots, m$ and $b \in \{0, 1\}$. The bit metrics of amplitude ($i \le n$) and phase ($n < i \le m$) for the SDD may be calculated according to their respective outputs as follows[1]:

$$\lambda^i(\gamma_k, \Delta\theta_k, b) = \begin{cases} \displaystyle\sum_{\{a_k, a_{k-1}\}_b^i} p(\gamma_k | a_k, a_{k-1}), & \text{for amplitude bits } (i \le n) \\ \displaystyle\sum_{\{\Delta\psi_k\}_b^i} p(\Delta\theta_k | \Delta\psi_k), & \text{for phase bits } (n < i \le m) \end{cases} \tag{3}$$

where $\{\boldsymbol{a}\}_b^i$ denotes the set of vector $\boldsymbol{a}$ with the ith coded bit labeling equal to b. In (3), knowledge of the conditional pdf's $p(\cdot|\cdot)$ may be necessary and their detailed derivations are placed in the Appendix.

With a little extra complexity, one may also incorporate the detected amplitude ratio γ_k to enhance the statistics of the phase bit metric. The resulting receiver is depicted in Fig. 3(b). We

[1]Whenever necessary, we assume that the noise variance σ^2 is estimated perfectly at the receiver.

refer to this approach as a *partially-combined differential detection* (PDD). In this case, the phase bit metric in (3) should be modified by replacing the corresponding pdf $p(\Delta\theta_k|\Delta\psi_k)$ with $p(\gamma_k, \Delta\theta_k|\Delta\psi_k)$.

The bit metrics are then processed by a binary channel decoder to make a hard decision. The following two decoding scenarios are considered.

1) Viterbi Decoding: The Viterbi decoding of BICM is performed by [15] and [16]

$$\hat{\boldsymbol{d}} = \underset{\boldsymbol{c}}{\operatorname{argmax}} \prod_t \lambda^i(\gamma_k, \Delta\theta_k, c_t) = \underset{\boldsymbol{c}}{\operatorname{argmax}} \sum_t \tilde{\lambda}^i(\gamma_k, \Delta\theta_k, c_t) \tag{4}$$

where $t = 0, 1, \ldots, N-1$ denotes the bit index before interleaving or after deinterleaving (i.e., the index at the stage of encoder/decoder) and $\tilde{\lambda}^i$ denotes a log-likelihood defined as

$$\tilde{\lambda}^i(\gamma_k, \Delta\theta_k, c_t) = \log \lambda^i(\gamma_k, \Delta\theta_k, c_t). \tag{5}$$

2) Iterative APP Decoding: For powerful class of channel coding such as turbo codes, the decoder typically employs the iterative APP algorithm. The APP decoder generates a hard decision and soft output in the form of the APP on the basis of the received sequence [19], [30]. It computes the log-likelihood ratio

$$\Lambda(\hat{d}_t) = \log \frac{p(\hat{d}_t = 1|\Delta\boldsymbol{\Theta}, \boldsymbol{\Gamma})}{p(\hat{d}_t = 0|\Delta\boldsymbol{\Theta}, \boldsymbol{\Gamma})} \tag{6}$$

for all t, where $\Delta\boldsymbol{\Theta}$ and $\boldsymbol{\Gamma}$ indicate the sequences of the differential detector outputs, i.e., $\Delta\boldsymbol{\Theta} = [\Delta\theta_1, \Delta\theta_2, \ldots, \Delta\theta_{N/m}]$ and $\boldsymbol{\Gamma} = [\gamma_1, \gamma_2, \cdots, \gamma_{N/m}]$. Finally, a hard decision $\hat{d}_t$ is made by

$$\hat{d}_t = \begin{cases} 0, & \text{if } \Lambda(\hat{d}_t) \le 0 \\ 1, & \text{otherwise} \end{cases}. \tag{7}$$

D. Maximum-Likelihood Differential Detection (MLDD)

In the case of MLDD, the ML metrics are calculated for each bit based on consecutive received symbols as illustrated in Fig. 3(c). In the case of two-symbol observation, the bit metric is given by

$$\lambda^i(Y_k, Y_{k-1}, b) = \sum_{\{X_k, X_{k-1}\}_b^i} p(Y_k, Y_{k-1}|X_k, X_{k-1}). \tag{8}$$

The major difference with the previous suboptimal detectors is the number of summations required for each bit metric calculation. Specifically, while the total number of bit metrics required for each symbol in the suboptimal system is given by $n \cdot 2^n + (m-n) \cdot 2^{m-n}$, that of MLDD is given by $m \cdot 2^{2m}$ since MLDD for DAPSK, even with a two-symbol observation, requires an averaging operation over all possible reference symbols [14]. In the case of 16-DAPSK with $n = 1$ and $m = 4$, MLDD requires calculation of 1024 bit metrics, while that of the suboptimal detection requires only 26.

III. Performance Analysis

In this section, we numerically calculate the AMI and cutoff rate of BICM-DAPSK systems on the basis of the assumption that the initial symbol X_k is chosen randomly from $\mathcal{X}$ with an equal probability, following the approach of [16] for the coherent case. The AMI may serve as a theoretical bound to the achievable information rate over the memoryless channel model defined in Section II-B. The cutoff rate is commonly used as a bench mark for the performance of convolutional codes despite the fact that it does not have any direct relation except for the case of sequential decoding [31]. However, as will be shown in the later section, the results of cutoff rate analysis and simulation show good agreement. Therefore, although empirical, we consider the cutoff rate as a useful design tool for estimating the performance of our system with Viterbi decoding.

The loss due to the use of suboptimal detectors comes in part from the lack of amplitude reference in the phase bit metric calculation. For the purpose of quantifying this loss, we introduce the following two ideal (and, thus practically infeasible) reference receivers.

1) **Perfect CSI receiver**: The CSI ρ_k is known at the receiver, which will be used for both phase and amplitude bit metric calculations.
2) **Genie-aided receiver**: The CSI ρ_k *and* the exactly transmitted amplitude pair $a_{k-1} = |X_{k-1}|$ and $a_k = |X_k|$ are known at the receiver, which will be used exclusively for phase bit metric calculation. The assumption of amplitude bit metric calculation is the same as that of the perfect CSI receiver above.

A. Average Mutual Information (AMI)

The AMI of BICM is expressed as a sum of the AMI of independent binary channels [16]. We evaluate the AMI of the amplitude bit and phase bit channels separately.

1) The SDD Case: For the amplitude bit channels ($i \le n$), the AMI after the DASK detector [see Fig. 3(a)] is given by

$$I\left(\gamma_k; \tilde{c}_k^i\right) = E_{\gamma_k, \tilde{c}_k^i}\left[\log_2\left(\frac{p\left(\gamma_k|\tilde{c}_k^i\right)}{p(\gamma_k)}\right)\right] \tag{9}$$

where $E_X[\cdot]$ denotes an expectation operation over a random variable X. The pdfs in (9) can be expressed as

$$p\left(\gamma_k|\tilde{c}_k^i\right) = E_{a_{k-1}}\left[E_{a_k|\tilde{c}_k^i, a_{k-1}}\left[p(\gamma_k|a_k, a_{k-1})\right]\right] \tag{10}$$

$$p(\gamma_k) = E_{a_k, a_{k-1}}\left[p(\gamma_k|a_k, a_{k-1})\right] \tag{11}$$

where $E_{X|Y}[\cdot]$ denotes a conditional expectation operation with respect to X given Y.

The total AMI achieved by the amplitude bit channels is given by

$$C_{\text{amp}} = \sum_{i=1}^{n} I\left(\gamma_k; \tilde{c}_k^i\right) \quad \text{(bits/symbol)}. \tag{12}$$

Also, the AMI achieved by the phase bit channels ($n < i \le m$) is given by

$$I\left(\Delta\theta_k; \tilde{c}_k^i\right) = E_{\Delta\theta_k, \tilde{c}_k^i}\left[\log_2\left(\frac{p\left(\Delta\theta_k|\tilde{c}_k^i\right)}{p(\Delta\theta_k)}\right)\right] \tag{13}$$

where

$$p\left(\Delta\theta_k|\tilde{c}_k^i\right) = E_{a_k, a_{k-1}}\left[E_{\Delta\psi_k|\tilde{c}_k^i, a_k, a_{k-1}}\left[p(\Delta\theta_k|a_k, a_{k-1}, \Delta\psi_k)\right]\right] \tag{14}$$

$$p(\Delta\theta_k) = E_{\Delta\psi_k, a_k, a_{k-1}}\left[p(\Delta\theta_k|a_k, a_{k-1}, \Delta\psi_k)\right]. \quad (15)$$

The total AMI of the phase bit channels is given by

$$C_{\text{phase}} = \sum_{i=n+1}^{m} I\left(\Delta\theta_k; \tilde{c}_k^i\right). \quad (16)$$

The overall AMI of the SDD without CSI is expressed as

$$C = C_{\text{amp}} + C_{\text{phase}}. \quad (17)$$

In general, the expectation operations above may not be expressed in a closed form, and we resort to numerical integration by the Monte Carlo method.

As a reference, if the CSI is available at the receiver, the AMI should be replaced by the corresponding *conditional* AMI and, thus, we have

$$C_{\text{amp}} = \sum_{i=1}^{n} I\left(\gamma_k; \tilde{c}_k^i|\rho_k\right) \quad (18)$$

$$C_{\text{phase}} = \sum_{i=n+1}^{m} I\left(\Delta\theta_k; \tilde{c}_k^i|\rho_k\right). \quad (19)$$

2) The PDD Case: The only difference with the SDD is its phase bit channel that now has the amplitude ratio information as observed from Fig. 3(b). Thus, without CSI we have

$$C_{\text{phase}} = \sum_{i=n+1}^{m} I\left(\Delta\theta_k; \tilde{c}_k^i|\gamma_k\right) \quad (20)$$

where the conditional AMI is expressed for $n < i \leq m$ as

$$I\left(\Delta\theta_k; \tilde{c}_k^i|\gamma_k\right) = E_{\Delta\theta_k, \gamma_k, \tilde{c}_k^i}\left[\log_2\left(\frac{p\left(\gamma_k, \Delta\theta_k|\tilde{c}_k^i\right)}{p(\gamma_k, \Delta\theta_k)}\right)\right]. \quad (21)$$

Also, if the CSI is available, the corresponding AMI for the phase bit channels becomes

$$C_{\text{phase}} = \sum_{i=n+1}^{m} I\left(\Delta\theta_k; \tilde{c}_k^i|\rho_k, \gamma_k\right). \quad (22)$$

3) Genie-Aided Receiver: The genie-aided receiver has a knowledge of the transmitted amplitude pair a_{k-1} and a_k, in addition to the received amplitude ratio γ_k, for the phase bit detection purpose. Thus, the AMI of the phase bit channels with this receiver can be expressed as

$$C_{\text{phase}} = \sum_{i=n+1}^{m} I\left(\Delta\theta_k; \tilde{c}_k^i|\rho_k, a_k, a_{k-1}, \gamma_k\right). \quad (23)$$

By assumption, C_{amp} of the genie-aided receiver is identical to that of the SDD with CSI, i.e., (18).

B. Cutoff Rate

The cutoff rate of BICM can be obtained from the Bhattacharyya bound on the average bit error probability P_b of the memoryless channel model defined in Section II-B in the absence of coding [16].

1) The SDD Case: For the cutoff rate of the SDD without CSI, we start with the channel transmitting a binary information by the amplitude ratio. By considering its metric calculation for the amplitude bits, the average bit error probability of this channel can be upper bounded as

$$P_{b,\text{amp}} \leq \frac{1}{n}\sum_{i=1}^{n} E_{\gamma_k, \tilde{c}_k^i}\left[\sqrt{\frac{p\left(\gamma_k|\overline{\tilde{c}_k^i}\right)}{p\left(\gamma_k|\tilde{c}_k^i\right)}}\right] \triangleq B_{\text{amp}} \quad (24)$$

where $\bar{c}$ denotes the change of state of c. The right-hand side term B_{amp} corresponds to the average Bhattacharyya factor of the binary channel, where the information is conveyed by the amplitude ratio [16], [32]. The corresponding cutoff rate of the amplitude bit channels may be written as

$$R_{0,\text{amp}} = n\left[1 - \log_2(B_{\text{amp}} + 1)\right]. \quad (25)$$

Likewise, the average bit error probability of the phase bit channels can be upper bounded as

$$P_{b,\text{phase}} \leq \frac{1}{(m-n)}\sum_{i=n+1}^{m} E_{\Delta\theta, \tilde{c}_k^i}\left[\sqrt{\frac{p\left(\Delta\theta_k|\overline{\tilde{c}_k^i}\right)}{p\left(\Delta\theta_k|\tilde{c}_k^i\right)}}\right] \triangleq B_{\text{phase}} \quad (26)$$

and the corresponding cutoff rate of the phase bit channels is

$$R_{0,\text{phase}} = (m-n)\left[1 - \log_2(B_{\text{phase}} + 1)\right]. \quad (27)$$

The cutoff rate of the overall channel with the SDD without CSI is expressed as

$$R_0 = R_{0,\text{amp}} + R_{0,\text{phase}}. \quad (28)$$

In the case where the perfect CSI is available, the corresponding average Bhattacharyya factor is given by

$$B_{\text{amp}} = \frac{1}{n}\sum_{i=1}^{n} E_{\gamma_k, \rho_k, \tilde{c}_k^i}\left[\sqrt{\frac{p\left(\gamma_k|\overline{\tilde{c}_k^i}, \rho_k\right)}{p\left(\gamma_k|\tilde{c}_k^i, \rho_k\right)}}\right] \quad (29)$$

$$B_{\text{phase}} = \frac{1}{(m-n)}\sum_{i=n+1}^{m} E_{\Delta\theta_k, \rho_k, \tilde{c}_k^i}\left[\sqrt{\frac{p\left(\Delta\theta_k|\overline{\tilde{c}_k^i}, \rho_k\right)}{p\left(\Delta\theta_k|\tilde{c}_k^i, \rho_k\right)}}\right]. \quad (30)$$

2) The PDD Case: Similar to the case of the AMI, the phase bit channels of the PDD incorporate statistics of amplitude ratio γ_k. Specifically, the average Bhattacharyya factor of the PDD without CSI is given by

$$B_{\text{phase}} = \frac{1}{(m-n)}\sum_{i=n+1}^{m} E_{\Delta\theta_k, \gamma_k, \tilde{c}_k^i}\left[\sqrt{\frac{p\left(\gamma_k, \Delta\theta_k|\overline{\tilde{c}_k^i}\right)}{p\left(\gamma_k, \Delta\theta_k|\tilde{c}_k^i\right)}}\right]. \quad (31)$$

Furthermore, if the perfect CSI is available, it can be expressed as

$$B_{\text{phase}} = \frac{1}{(m-n)} \sum_{i=n+1}^{m} E_{\Delta\theta_k,\gamma_k,\rho_k,\tilde{c}_k^i} \left[\sqrt{\frac{p\left(\gamma_k, \Delta\theta_k | \overline{\tilde{c}_k^i}, \rho_k\right)}{p\left(\gamma_k, \Delta\theta_k | \tilde{c}_k^i, \rho_k\right)}} \right]. \tag{32}$$

3) Genie-Aided Receiver: With genie-aided receiver for the phase bit channels, we obtain

$$B_{\text{phase}} = \frac{1}{(m-n)} \sum_{i=n+1}^{m} E_{\Delta\theta_k,\gamma_k,\rho_k,a_k,a_{k-1},\tilde{c}_k^i} \left[\sqrt{\frac{p\left(\gamma_k, \Delta\theta_k | \overline{\tilde{c}_k^i}, \rho_k, a_k, a_{k-1}\right)}{p\left(\gamma_k, \Delta\theta_k | \tilde{c}_k^i, \rho_k, a_k, a_{k-1}\right)}} \right]. \tag{33}$$

C. Numerical Results

1) Average Mutual Information Results: Fig. 4(a) shows the AMI of BICM with 16-DAPSK ($n = 1$, $m = 4$, $\alpha = 2.0$) constellation in conjunction with the suboptimal SDD and PDD without CSI, perfect CSI, and the genie-aided receivers. As a reference, the AMI of DAPSK with MLDD without CSI [14], as well as that of bit-interleaved 16-QAM with coherent reception and perfect CSI is illustrated [16].

It follows from the data processing inequality [33] that the AMI of MLDD is always larger than that of any other suboptimal differential detection, and the AMI of the PDD should be always larger than that of the SDD. Similarly, the AMI of the genie-aided receiver is always larger than that of the suboptimal detector with perfect CSI. These relations can be observed in Fig. 4(a).

From the figure, it is apparent that the loss of the suboptimal detectors due to the lack of CSI is considerable, whereas the AMI of the genie-aided receiver is close to that of MLDD. Thus, it can be conjectured that the superiority of MLDD comes from the fact that MLDD uses both amplitude and phase statistics to calculate each bit metric, whereas the suboptimal detectors for DAPSK signaling calculate amplitude and phase metrics independently. The removal of this statistical correlation results in the loss of achievable AMI, which could be retrieved significantly with the genie-aided receiver.

2) Cutoff Rate Results: Fig. 4(b) shows the cutoff rate of BICM with 16-DAPSK ($n = 1$, $m = 4$, $\alpha = 2.0$) constellation for the suboptimal detectors with and without CSI, as well as the genie-aided receiver. As a reference, the cutoff rates of MLDD without CSI [9] and bit-interleaved 16-QAM with coherent reception and perfect CSI [16] are shown. Clearly, strong similarity to the AMI case is observed. The cutoff rate of MLDD is always larger than that of suboptimal detectors, and the PDD is always superior to the SDD. It is interesting to note that unlike the AMI case, the genie-aided receiver almost achieves the same value of the cutoff rate as MLDD.

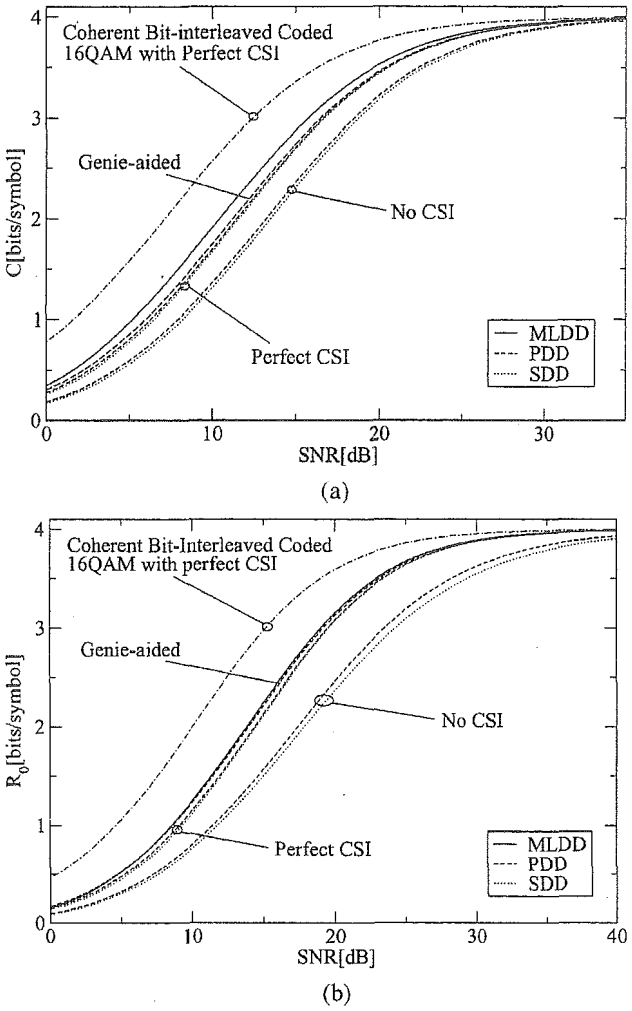

Fig. 4. Comparison of 16-level BICM over frequency nonselective Rayleigh-fading channels. (a) Average mutual information results. (b) Cutoff rate results.

IV. New Bit Metrics for BICM-DAPSK Over Raleigh-Fading Channels

The comparative studies on the AMI and cutoff rate in the previous section suggest that the performance gap between MLDD and suboptimal detectors without CSI in terms of the required SNR to achieve a certain information rate is noticeable. In other words, ignoring the knowledge of received amplitude information, composed of both CSI and transmitted amplitude, may significantly reduce the achievable information rate for a given SNR. Thus, if one can restore these information from the received symbol, it may improve the performance dramatically. Therefore, we wish to find a new bit metric that can approach the performance with the *genie-aided* receiver by suitably incorporating information from the detector. In fact, as proposed in [19], the output of the envelope detector can be used for this purpose. However, the metric proposed in [19] is based on the empirical Gaussian approximation of the associated pdf. In the following, we develop improved bit metrics for the Viterbi and iterative APP decoders based on the *exact* pdf's derived in the Appendix.

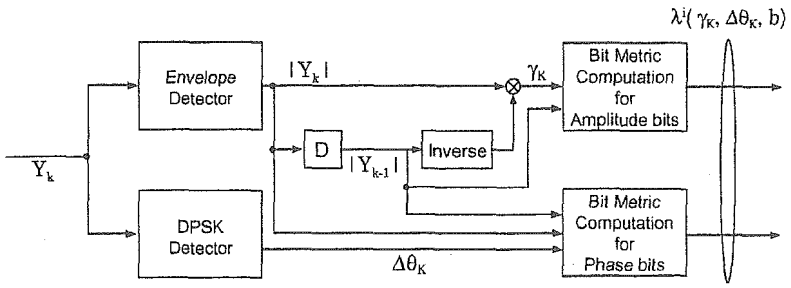

Fig. 5. Block diagram of the proposed receiver.

A. Bit Metrics for the Viterbi Decoder

1) Bit Metric for Amplitude: We first derive a bit metric for amplitude bits that can be used for convolutional codes with a Viterbi decoder. For the purpose mentioned above, we start with the bit metrics of the suboptimal detectors with CSI. Recall that the Viterbi decoder utilizes the bit metric given in (4), where for CSI case, the log-likelihood $\tilde{\lambda}^i(\gamma_k, \Delta\theta_k, c_t)$ should be replaced by $\tilde{\lambda}^i(\gamma_k, \Delta\theta_k, c_t|\rho_k)$. From (3), the computation of the metric requires the associated conditional pdf $p(\gamma_k|a_k, a_{k-1}, \rho_k)$. This is derived in (49) in the Appendix.

Unfortunately, direct application of (49) into bit metric calculation is quite complicated, since the calculation of the Bessel function is necessary. Furthermore, the knowledge of noise variance σ^2 is required. Thus, we first utilize an exponent-form approximation of the Bessel function as

$$I_n(x) \approx \frac{1}{\sqrt{2\pi x}} \exp[x]. \tag{34}$$

The above approximation may become accurate for $x \gg n$ [34], and in our scenario this is the case for high SNR. Then, (49) can be rewritten as

$$\begin{aligned} &p(\gamma_k|a_k, a_{k-1}, \rho_k) \\ &\approx \frac{1}{(1+\gamma_k^2)^{\frac{5}{2}} \sqrt{2\pi\sigma^2\rho_k^2 a_k a_{k-1}\gamma_k}} \\ &\quad \times \left\{2\gamma_k\sigma^2\left(1+\gamma_k^2\right) + \gamma_k\rho_k^2(a_k\gamma_k + a_{k-1})^2\right\} \\ &\quad \cdot \exp\left[\frac{-\rho_k^2}{2\sigma^2(1+\gamma_k^2)}(a_k - a_{k-1}\gamma_k)^2\right]. \end{aligned} \tag{35}$$

Furthermore, for high SNR, the log-sum approximation $\log\sum_j z_j \approx \max_j \log z_j$ becomes accurate since in this case the summation in the left-hand side is dominated by the single maximum term [15]. Also, multiplication of (35) by $2\sigma^2$ after log-sum approximation does not change the maximization in the Viterbi decoding. Thus, with all the above manipulations and dropping constant terms that do not affect the maximization, the log-likelihood can be expressed as

$$\tilde{\lambda}^i(\gamma_k, \Delta\theta_k, b|\rho_k) \approx \max_{\{a_k, a_{k-1}\}_b^i} \left[-\frac{\rho_k^2}{(1+\gamma_k^2)}(a_k - a_{k-1}\gamma_k)^2\right]. \tag{36}$$

Furthermore, inducing the approximation of CSI with the received sample amplitude as

$$\rho_k a_k \approx |Y_k| \tag{37}$$

which also becomes accurate for high SNR [19], we obtain

$$\tilde{\lambda}^i(\gamma_k, \Delta\theta_k, b|\rho_k) \approx \max_{\hat{r}_{b,k}^i} \left[\frac{-|Y_{k-1}|^2}{(1+\gamma_k^2)}\left(\gamma_k - \hat{r}_{b,k}^i\right)^2\right] \tag{38}$$

where $\hat{r}_k$ is defined as $\hat{r}_k = a_k/a_{k-1}$. Note that the above bit metric exploits the envelope detector output $|Y_{k-1}|$, and the resulting receiver structure may be depicted as in Fig. 5. The increase of detector complexity by this additional operation may be minor in practice.

2) Bit Metric for Phase: The cutoff rate results suggest that the received amplitude ratio γ_k or the output of envelope detector should be used in bit metric calculation. Therefore, by using $p(\gamma_k, \Delta\theta_k|a_k, a_{k-1}, \Delta\psi_k, \rho_k)$ of (43) in the Appendix and applying the same approximation procedure as for the amplitude bit metric, we may write the phase bit metric in an approximate form as

$$\begin{aligned} \tilde{\lambda}^i(\gamma_k, \Delta\theta_k, b|\rho_k, a_k, a_{k-1}) &\approx \max_{\Delta\psi_{b,k}^i} \\ &\times \left[\frac{|Y_k||Y_{k-1}|\gamma_k}{1+\gamma_k^2}\cos\left(\Delta\theta_k - \Delta\psi_{b,k}^i\right)\right]. \end{aligned} \tag{39}$$

In the following simulation, we will make use of (38) and (39) for bit metric calculation. The receiver structure for this case is also illustrated in Fig. 5.

B. Bit Metric for Iterative APP Decoder

For the APP decoder, simple and practical bit metrics can be derived from the exact pdfs. With the approximate pdf (35) and similar approximation procedures above, the amplitude bit metric can be obtained as

$$\begin{aligned} &\lambda^i(\gamma_k, \Delta\theta_k, c_t|\rho_k) \\ &\approx \sum_{\hat{r}_{b,k}^i} \frac{2\gamma_k\sigma^2\left(1+\gamma_k^2\right) + \gamma_k|Y_{k-1}|^2(\hat{r}_k\gamma_k + 1)^2}{(1+\gamma_k^2)^{\frac{5}{2}}\sqrt{2\pi\sigma^2|Y_{k-1}|^2\hat{r}\gamma_k}} \\ &\quad \times \exp\left[\frac{-|Y_{k-1}|^2}{2\sigma^2(1+\gamma_k^2)}(\gamma_k - \hat{r}_k)^2\right]. \end{aligned} \tag{40}$$

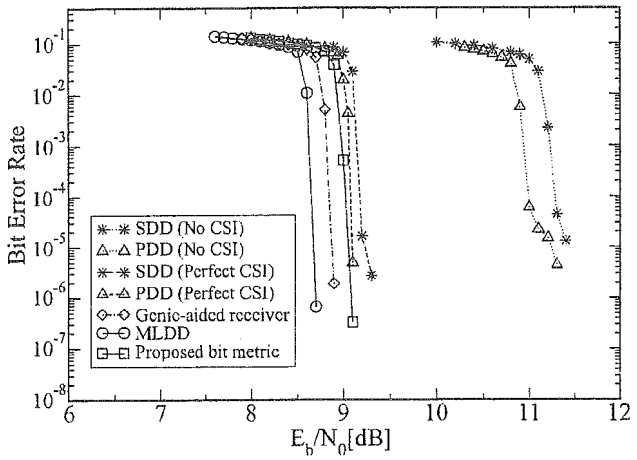

Fig. 6. Comparison of the bit metrics for iterative APP decoding and rate 1/2 turbo codes.

Likewise, an approximate form of the phase bit metric can be obtained from (43) in the Appendix as

$$\lambda^i(\gamma_k, \Delta\theta_k, c_t|\rho_k) \approx \sum_{\Delta\psi^i_{k,b}} \frac{\gamma_k}{\pi(1+\gamma_k^2)^2} \times \left[1+\frac{1}{2\sigma^2(1+\gamma_k^2)}\{|Y_k|^2\gamma_k^2+|Y_{k-1}|^2+2\gamma_k|Y_k||Y_{k-1}| \times \cos(\Delta\theta_k-\Delta\psi_k)\}\right] \cdot \exp\left[-\frac{1}{2\sigma^2(1+\gamma_k^2)}\{|Y_k|^2+|Y_{k-1}|^2\gamma_k^2-2|Y_k| \times|Y_{k-1}|\gamma_k\cos(\Delta\theta_k-\Delta\psi_k)\}\right]. \quad (41)$$

The approximate bit metrics derived above are practically attractive, since they neither require CSI nor include any special function such as Bessel functions.

V. Simulation Results

In this section, the bit-error performance of the proposed receiver is compared with those of the other receiver structures discussed in the previous sections based on computer simulations using turbo and convolutional codes.

A. Differential Detection With Iterative APP Decoder

A turbo code with interleaver size 120 000 is chosen as a channel encoder. The coding rate of the turbo code is made 1/2 by puncturing [35]. The component code is the rate 1/2 recursive systematic convolutional code (37,21) in octal form. The number of iteration for iterative APP decoding is 18. Furthermore, an ideal bit interleaver is assumed [15].

Fig. 6 shows the bit-error rate (BER) versus SNR per information bit E_b/N_0, where E_b is the average received energy per information bit and N_0 is one-sided power spectral density of the AWGN. These simulation results show good agreement with the AMI values in Fig. 4(a). The comparisons of the required minimum E_b/N_0 for achieving a BER of 10^{-4} and the corresponding values of AMI are listed in Table I.

TABLE I
REQUIRED E_b/N_0 TO ACHIEVE AMI $C = 2.0$ BITS/SYMBOL AND BER $= 10^{-4}$ WITH RATE 1/2 TURBO CODES OVER RAYLEIGH-FADING CHANNELS

Receiver	AMI Results [dB]	Simulation Results [dB]
MLDD	7.4	8.6
PDD (Genie-aided)	8.2	8.8
Proposed bit metric	—	9.0
PDD (Perfect CSI)	8.5	9.1
SDD (Perfect CSI)	8.6	9.2
PDD (No CSI)	10.2	11.0
SDD (No CSI)	10.5	11.3

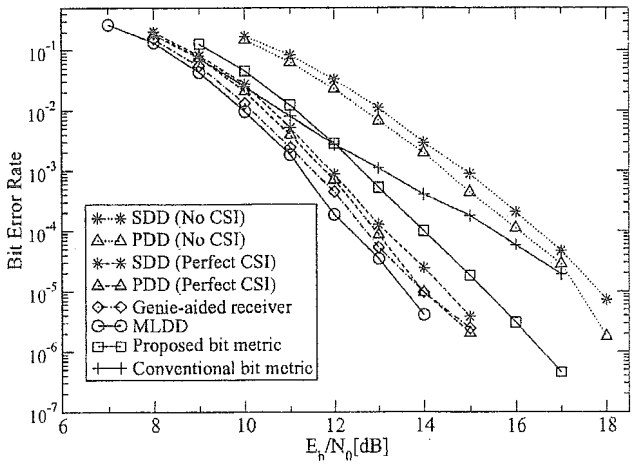

Fig. 7. Comparison of the bit metrics for Viterbi decoder with rate 1/2 convolutional codes.

As observed, the performance loss of the suboptimal detector with the proposed metric with respect to the genie-aided receiver is less than 0.2 dB, and even within 0.5 dB of that of MLDD. Therefore, considering the low-complexity, suboptimal detection with the proposed metric may be an attractive alternative for MLDD.

B. Differential Detection With Viterbi Decoder

The bit-error performance of bit-interleaved 16-DAPSK with Viterbi decoding employing the proposed metric, together with the other suboptimal metrics and MLDD, has been also evaluated by simulation. The rate-1/2 convolutional code is used with information size 65 536, generation matrix (133 171) in octal form, and constraint length $K = 7$. An ideal bit interleaver is assumed.

Fig. 7 shows the BER versus E_b/N_0 over frequency nonselective Rayleigh-fading channels. The performance of the metric proposed in [20] is also shown as "conventional bit metric" in Fig. 7 for comparison. First, it is worth mentioning that the theoretical performance analysis results presented in Section III-C2 are in good agreement with the simulation results. Similar to the turbo code results, the comparisons of simulation and corresponding cutoff rate results are listed in Table II. Again, the required minimum E_b/N_0 is calculated at a BER of 10^{-4} for simulations.

TABLE II
REQUIRED E_b/N_0 TO ACHIEVE CUTOFF RATE $R_0 = 2.0$ BITS/SYMBOL AND BER $= 10^{-4}$ WITH RATE 1/2 CONVOLUTIONAL CODES OVER RAYLEIGH-FADING CHANNELS

Receiver	Cutoff Rate Results [dB]	Simulation Results [dB]
MLDD	10.8	12.4
PDD (Genie-aided)	11.0	12.7
PDD (Perfect CSI)	11.4	12.9
SDD (Perfect CSI)	11.5	13.1
Proposed bit metric	——	14.0
Conventional bit metric	——	15.5
PDD (No CSI)	14.4	16.1
SDD (No CSI)	14.9	16.5

As observed, the gap between the proposed metric and genie-aided receiver is still noticeable. This gap may stem mainly from the approximation associated with noise variance σ^2 for the bit metric simplification. Nevertheless, it is observed that the proposed bit metric can significantly outperform that of [19] for a high SNR region, still retaining a simple receiver structure.

VI. CONCLUSION

In this paper, we have studied the performance of low-complexity bit-interleaved coded DAPSK over frequency nonselective Rayleigh-fading channels based on separate demodulation and decoding scenario. We have derived the exact bit metrics of the suboptimal detectors such as the SDD and PDD and made comparison with MLDD in terms of AMI and cutoff rate. The exact pdfs of the detector outputs have been derived for this purpose. The numerical results have shown quantitatively that the theoretical performance loss due to the use of the suboptimal detectors is considerable. In order to mitigate this gap, a new bit metric in conjunction with the suboptimal detector has been proposed based on the exact pdfs developed in this paper. Simulation results have shown that the proposed metric can improve performance significantly without noticeable increase of receiver complexity.

Finally, throughout this paper, we have focused on DAPSK only with BICM exclusively for simplicity. However, our results can readily be extended to MLC, which may result in improved performance, if properly designed, in accordance with [9] and [14].

APPENDIX I
DERIVATION OF PROBABILITY DENSITIES FUNCTIONS

In this Appendix, we derive the exact pdfs of the amplitude ratio γ_k and phase difference $\Delta\theta_k$ for given channel statistics. These results are used for calculating the bit metrics and associated AMI and cutoff rate in this paper.

A. Probability Density Function (pdf) Without CSI

We start with the derivation of the pdf in the absence of CSI ρ_k.

1) Amplitude Ratio: Given that two consecutive symbols X_{k-1} and X_k are transmitted, the conditional joint pdf of the two received consecutive symbols is given by

$$p(Y_k, Y_{k-1}|X_k, X_{k-1}, \rho_k, \rho_{k-1}, \phi_k, \phi_{k-1}) = \frac{1}{(2\pi\sigma^2)^2} \times \exp\left[-\frac{1}{2\sigma^2}\left(|Y_k - \rho_k X_k e^{j\phi_k}|^2 + |Y_{k-1} - \rho_{k-1} X_{k-1} e^{j\phi_{k-1}}|^2\right)\right]. \quad (42)$$

With the channel model in Section II-B in mind and changing the variables appropriately, we obtain (see, e.g., [36])

$$p(\gamma_k, \Delta\theta_k|a_k, a_{k-1}, \Delta\psi_k, \rho_k) = \frac{\gamma_k}{\pi\left(1+\gamma_k^2\right)^2} \times \left[1 + \frac{\rho_k^2}{2\sigma^2\left(1+\gamma_k^2\right)} \times \left\{a_k^2\gamma_k^2 + a_{k-1}^2 + 2\gamma_k a_k a_{k-1}\cos(\Delta\theta_k - \Delta\psi_k)\right\}\right] \cdot \exp\left[-\frac{\rho_k^2}{2\sigma^2\left(1+\gamma_k^2\right)}\left\{a_k^2 + a_{k-1}^2\gamma_k^2 - 2a_k a_{k-1}\gamma_k \times \cos(\Delta\theta_k - \Delta\psi_k)\right\}\right] \quad (43)$$

where $a_k = |X_k|$. Integrating out ρ_k in (43), we obtain (44), as shown at bottom of page. Similarly, integrating out $\Delta\theta_k$ in the above equation, we obtain (45), as shown at bottom of page, where

$$z_k \triangleq \left(1 - \frac{4a_k a_{k-1}\gamma_k}{a_k^2 + 2\sigma^2 + 2a_k a_{k-1}\gamma_k + \left(a_{k-1}^2 + 2\sigma^2\right)\gamma_k^2}\right)^{\frac{3}{2}}. \quad (46)$$

$$p(\gamma_k, \Delta\theta_k|a_k, a_{k-1}, \Delta\psi_k) = \frac{2\sigma^2\left(a_k^2 + a_{k-1}^2 + 2\sigma^2\right)\gamma_k}{\pi\left(a_k^2 + 2\sigma^2 + \left(a_{k-1}^2 + 2\sigma^2\right)\gamma_k^2 - 2a_k a_{k-1}\gamma_k\cos(\Delta\theta_k - \Delta\psi_k)\right)^2} \quad (44)$$

$$p(\gamma_k|a_k, a_{k-1}) = \frac{4\sigma^2\gamma_k\left\{a_k^2 + a_{k-1}^2 + 2\sigma^2\right\}\left\{a_k^2 + 2\sigma^2 + \left(a_{k-1}^2 + 2\sigma^2\right)\gamma_k^2\right\}}{z_k \cdot \left\{a_k^2 + 2\sigma^2 + 2a_k a_{k-1}\gamma_k + \left(a_{k-1}^2 + 2\sigma^2\right)\gamma_k^2\right\}^3} \quad (45)$$

2) Phase Difference: The pdf of the phase difference between two consecutive DAPSK modulated symbols can be obtained by integrating out γ_k in (44), yielding

$$p(\Delta\theta_k|a_k, a_{k-1}, \Delta\psi_k) = \frac{\sigma^2\left(a_k^2 + a_{k-1}^2 + 2\sigma^2\right)}{\pi\xi_k\left(a_{k-1}^2 + 2\sigma^2\right)} \times \left\{2\left(a_{k-1}^2 + 2\sigma^2\right) + a_k a_{k-1}\cos(\Delta\theta_k - \Delta\psi_k)\cdot\Lambda_k\right\} \quad (47)$$

where

$$\begin{aligned}\Lambda_k &\triangleq \frac{1}{\eta_k} 2\left(a_{k-1}^2+2\sigma^2\right)\arctan\left[\frac{a_k a_{k-1}\cos(\Delta\theta_k-\Delta\psi_k)}{\eta_k}\right] \\ &\quad + \pi\left(a_{k-1}^2+2\sigma^2\right) \\ \eta_k &\triangleq \sqrt{\left(a_k^2+2\sigma^2\right)\left(a_{k-1}^2+2\sigma^2\right) - a_k^2 a_{k-1}^2\cos(\Delta\theta_k-\Delta\psi_k)^2} \\ \xi_k &\triangleq 4\sigma^2\left(a_{k-1}^2+2\sigma^2\right)+a_k^2\left(a_{k-1}^2+4\sigma^2\right) \\ &\quad - a_k^2 a_{k-1}^2\cos\left[2(\Delta\theta_k-\Delta\psi_k)\right]. \end{aligned} \quad (48)$$

B. Probability Density Function (pdf) With CSI

1) Amplitude Ratio: As a reference, if CSI ρ_k is known at the receiver, the corresponding pdf can be obtained by integrating out $\Delta\theta_k$ in (43). The result is expressed as

$$\begin{aligned} p(\gamma_k|a_k, a_{k-1}, \rho_k) &= \frac{2\gamma_k}{\left(1+\gamma_k^2\right)^2}\exp\left[-\frac{\rho_k^2}{2\sigma^2\left(1+\gamma_k^2\right)}\left\{a_k^2 + a_{k-1}^2\gamma_k^2\right\}\right] \\ &\quad\times I_0\left(\frac{\rho_k^2 a_k a_{k-1}\gamma_k}{\sigma^2\left(1+\gamma_k^2\right)}\right) + \frac{\gamma_k\rho_k^2}{\sigma^2\left(1+\gamma_k^2\right)^3}\left(a_k^2\gamma_k^2 + a_{k-1}^2\right) \\ &\quad\times\exp\left[-\frac{\rho_k^2}{2\sigma^2\left(1+\gamma_k^2\right)}\left\{a_k^2 + a_{k-1}^2\gamma_k^2\right\}\right] \\ &\quad\times I_0\left(\frac{\rho_k^2 a_k a_{k-1}\gamma_k}{\sigma^2\left(1+\gamma_k^2\right)}\right) + \frac{2\gamma_k^2\rho_k^2 a_k a_{k-1}}{\sigma^2\left(1+\gamma_k^2\right)^3} \\ &\quad\times\exp\left[-\frac{\rho_k^2}{2\sigma^2\left(1+\gamma_k^2\right)}\left\{a_k^2 + a_{k-1}^2\gamma_k^2\right\}\right] \\ &\quad\times I_1\left(\frac{\rho_k^2 a_k a_{k-1}\gamma_k}{\sigma^2\left(1+\gamma_k^2\right)}\right) \end{aligned} \quad (49)$$

where $I_n(\cdot)$ is the modified Bessel function of the first kind with order n [34].

2) Phase Difference: The pdf of the phase difference may not be expressed in a closed form directly from (43). An alternative solution is the use of characteristic function (see, e.g., [37]–[41]), which may result in

$$\begin{aligned} p(\Delta\theta_k|a_k, a_{k-1}, \Delta\psi_k, \rho_k) &= \frac{1}{4\pi}\int_0^\pi \sin\alpha\left[1 + U_k + V_k\cos\alpha\right. \\ &\qquad \left. + W_k\sin\alpha\cos(\Delta\theta_k - \Delta\psi_k)\right] \\ &\quad\cdot\exp\left[V_k\cos\alpha\right. \\ &\qquad \left. + W_k\sin\alpha\cos(\Delta\theta_k - \Delta\psi_k) - U_k\right] d\alpha \end{aligned} \quad (50)$$

where

$$U_k = \frac{\rho_k^2}{4\sigma^2}\left(a_k^2 + a_{k-1}^2\right),\ V_k = \frac{\rho_k^2}{4\sigma^2}\left(a_k^2 - a_{k-1}^2\right),\ W_k = U_k^2 - V_k^2. \quad (51)$$

Furthermore, (50) can be simplified as [42]

$$p(\Delta\theta_k|a_k, a_{k-1}, \Delta\psi_k, \rho_k) = \frac{e^{-U_k}}{2\pi}\cosh V_k + \frac{1}{4\pi}\int_0^\pi e^{-Z_k}\left[W_k\cos(\Delta\theta_k - \Delta\psi_k) + U_k\sin\alpha\right] d\alpha \quad (52)$$

where

$$Z_k = U_k - V_k\cos\alpha - W_k\sin\alpha\cos(\Delta\theta_k - \Delta\psi_k). \quad (53)$$

Further simplification of (52) appears to be difficult to carry out and thus one may resort to numerical integration.

ACKNOWLEDGMENT

The authors wish to thank R. F. Pawula for his valuable comments, especially with respect to the derivation of Appendix I-B2, and the editor and anonymous reviewers for their comments that improved the quality of manuscript.

REFERENCES

[1] H. Rohling and V. Engels, "Differential amplitude phase shift keying (DAPSK)—A new modulation method for DTVB," in *Proc. Int. Broadcasting Convention*, Amsterdam, The Netherlands, 1995, pp. 102–108.
[2] H. Leib and S. Pasupathy, "The phase of a vector perturbed by Gaussian noise and differentially coherent receivers," *IEEE Trans. Inf. Theory*, vol. 34, no. 6, pp. 1491–1501, Nov. 1988.
[3] D. Makrakis and P. T. Mathiopoulos, "Trellis coded noncoherent QAM: A new bandwidth and power efficient scheme," in *Proc. IEEE VTC*, San Francisco, CA, May 1989, pp. 95–100.
[4] S. G. Wilson, J. Freebersyser, and C. Marshall, "Multisymbol differential detection of MPSK," in *Proc. IEEE GLOBECOM*, Dallas, TX, Nov. 1989, pp. 1692–1697.
[5] D. Divsalar and M. K. Simon, "Multiple-symbol differential detection of MPSK," *IEEE Trans. Commun.*, vol. 38, no. 3, pp. 300–308, Mar. 1990.
[6] P. Y. Kam and C. H. Teh, "Reception of PSK signals over fading channels via quadrature amplitude estimation," *IEEE Trans. Commun.*, vol. 31, no. 8, pp. 1024–1027, Aug. 1983.
[7] A. Svensson, "Coherent detection based on linear prediction and decision feedback for QDPSK," *Electron. Lett.*, vol. 30, pp. 1642–1643, Aug. 1994.
[8] R. Schober, W. H. Gerstacker, and J. B. Huber, "Decision-feedback differential detection of MDPSK for flat Rayleigh-fading channels," *IEEE Trans. Commun.*, vol. 47, no. 7, pp. 1025–1035, Jul. 1999.
[9] L. Lampe, "Noncoherent coded modulation," Ph.D. dissertation, Universität Erlangen–Nürnberg, Erlangen, Germany, 1999.
[10] ——, "Multiple-symbol differential sphere decoding," in *Proc. IEEE ICC*, Paris, France, Jun. 2004, pp. 787–791.
[11] G. Ferrari, A. Anastasopoulos, G. Colavolpe, and R. Raheli, "Adaptive iterative detection for the phase-uncertain channel: Limited-tree-search versus truncated-memory detection," *IEEE Trans. Veh Technol.*, vol. 53, no. 2, pp. 433–442, Mar. 2004.
[12] M. Peleg, S. Shamai(Shitz), and S. Galan, "On iterative decoding for coded noncoherent MPSK communications over phase noisy AWGN channel," in *Proc. Inst. Elect. Eng.-Commun.*, vol. 147, Apr. 2000, pp. 87–95.
[13] W. T. Webb, L. Hanzo, and R. Steele, "Bandwidth efficient QAM schemes for Rayleigh-fading channels," *Proc. I, Commun., Speech, Vision,—IEE*, vol. 138, no. 3, pp. 169–175, Jun. 1991.
[14] R. F. H. Fischer, L. H.-J. Lampe, and S. H. Muller-Weinfürtner, "Coded modulation for noncoherent reception with application to OFDM," *IEEE Trans. Veh Technol.*, vol. 50, no. 4, pp. 901–919, Jul. 2001.
[15] E. Zehavi, "8-PSK trellis codes for a Rayleigh channel," *IEEE Trans. Commun.*, vol. 40, no. 5, pp. 873–884, May 1992.
[16] G. Caire, G. Taricco, and E. Biglieri, "Bit-interleaved coded modulation," *IEEE Trans. Inf. Theory*, vol. 44, no. 3, pp. 927–946, May 1998.
[17] H. Imai and S. Hirakawa, "A new multilevel coding method using error-correcting codes," *IEEE Trans. Inf. Theory*, vol. 23, no. 3, pp. 371–377, May 1977.

[18] U. Wachsmann, R. F. H. Fischer, and J. B. Huber, "Multilevel codes: Theoretical concepts and practical design rules," *IEEE Trans. Inf. Theory*, vol. 45, no. 5, pp. 1361–1391, Jul. 1999.
[19] T. May, H. Rohling, and V. Engels, "Performance analysis of Viterbi decoding for 64-DAPSK and 64-QAM modulated OFDM signals," *IEEE Trans. Commun.*, vol. 46, no. 2, pp. 182–190, Feb. 1998.
[20] Y. Kofman, E. Zehavi, and S. Shamai(Shitz), "nd-convolutional codes—Part I: Performance analysis," *IEEE Trans. Inf. Theory*, vol. 43, no. 2, pp. 558–575, Mar. 1997.
[21] G. Kaplan and S. Shamai(Shitz), "On the achievable information rates of DPSK," *Proc.—I, IEE* , vol. 139, pp. 311–318, Jun. 1992.
[22] M. Peleg and S. Shamai(Shitz), "On the capacity of the blockwise incoherent MPSK channel," *IEEE Trans. Commun.*, vol. 46, no. 5, pp. 603–609, May 1998.
[23] G. Colavolpe and R. Raheli, "The capacity of the noncoherent channel," *Eur. Trans. Telecomm.(ETT)*, vol. 12, no. 4, pp. 603–609, Jul.–Aug. 2001.
[24] S. I. Chen and T. Fuja, "Channel capacity and cutoff rates for DPSK on fading channels," in *Conf. Inf. Sci. Systems*, vol. 1, Princeton, NJ, 1996, pp. 375–380.
[25] F. Adachi and M. Sawahashi, "Performance analysis of various 16 level modulation schemes under Rayleigh fading," *Electron. Lett.*, vol. 28, no. 17, pp. 1579–1581, Aug. 1992.
[26] L. H.-J. Lampe and R. F. H. Fischer, "Comparison and optimization of differentially encoded transmission on fading channels," in *Proc. Int. Symp. Powerline Commun. Applicat.*, Lancaster, U.K., 1999, pp. 107–113.
[27] L. Ozarow, S. Shamai(Shitz), and A. D. Wyner, "Information theoretic considerations for cellular mobile radio," *IEEE Trans. Veh Technol.*, vol. 43, no. 2, pp. 359–378, May 1994.
[28] J. Ventura-Traveset, G. Caire, E. Biglieri, and G. Taricco, "Impact of diversity reception on fading channels with coded modulation—Part II: Differential block detection," *IEEE Trans. Commun.*, vol. 45, pp. 676–686, Jun. 1997.
[29] E. Malkamäki and H. Leib, "Coded diversity on block-fading channels," *IEEE Trans. Inf. Theory*, vol. 45, no. 2, pp. 771–782, Mar. 1999.
[30] S. LeGoff, A. Glavieux, and C. Berrou, "Turbo codes and high efficiency modulation," in *Proc. IEEE ICC*, New Orleans, LA, May 1994, pp. 645–649.
[31] A. J. Viterbi and J. K. Omura, *Principles of Digital Communication and Coding*. Cambridge, MA: MIT Press, 1979.
[32] S. G. Wilson, *Digital Modulation and Coding*. Englewood Cliffs, NJ: Prentice-Hall, 1996.
[33] R. G. Gallager, *Information Theory and Reliable Communication*. New York: Wiley, 1968.
[34] W. H. Press, S. A. Teukolsky, W. T. Vetterling, and B. P. Flannery, *Numerical Recipes in C: The Art of Scientific Computing*, 2nd ed. Cambridge, U.K.: Cambridge Univ. Press, 1992.
[35] C. Berrou, A. Glavieux, and P. Thitimajshima, "Near Shannon limit error-correcting coding and decoding: Turbo-codes," in *Proc. IEEE ICC*, Geneva, Switzerland, May 1993, pp. 1064–1070.
[36] T. Suzuki and T. Mizuno, "Multiple-symbol differential detection scheme for differential amplitude modulation," in *Proc. Int. Zurich Seminar Digital Commun.*, Zurich, Switzerland, 1994, pp. 326–337.
[37] R. F. Pawula, "On the theory of error rates for narrowband digital FM," *IEEE Trans. Commun.*, vol. COM-29, pp. 1634–1643, Nov. 1981.
[38] R. F. Pawula, S. O. Rice, and J. H. Roberts, "Distribution of the phase angle between two vectors perturbed by Gaussian noise," *IEEE Trans. Commun.*, vol. COM-30, no. 8, pp. 1828–1841, Aug. 1982.
[39] R. F. Pawula, "Distribution of the phase angle between two vectors perturbed by Gaussian noise II," *IEEE Trans. Veh. Technol.*, vol. 50, no. 2, pp. 576–583, Mar. 2001.
[40] J. G. Proakis, *Digital Communications*, 4th ed. New York: McGraw-Hill, 2001.
[41] W. C. Lindsey and M. K. Simon, *Telecommunication Systems Engineering*. Englewood Cliffs, NJ: Prentice-Hall, 1973.
[42] R. F. Pawula, private communication, Apr. 2004.

Koji Ishibashi (S'01) was born in Kofu, Yamanashi, Japan, in May 1979. He received the B.E. and M.E. degrees in engineering from the University of Electro-Communications, Tokyo, Japan, in 2002 and 2004, respectively. He is currently working towards the Ph.D. degree at Yokohama National University, Kanagawa, Japan.

His current interests are coded modulation, differential detection, and information theory.

He is a Student Member of IEEE Communications, Information Theory and Vehicular Technology Society. He is also a member of Institute of Electrical, Information, and Communication Engineers (IEICE) and SITA, Japan.

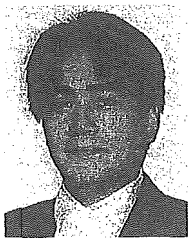

Hideki Ochiai (S'97–M'01) received the B.E. degree in communication engineering from Osaka University, Osaka, Japan, in 1996, and the M.E. and Ph.D. degrees in information and communication engineering from the University of Tokyo, Tokyo, Japan, in 1998 and 2001, respectively.

From 1994 to 1995, he was with the Department of Electrical Engineering, University of California, Los Angeles, under the scholarship of the Ministry of Education, Science, and Culture. From 2001 to 2003, he was a Research Associate at the Department of Information and Communication Engineering, University of Electro-Communications, Tokyo, Japan. Since April 2003, he has been with the Department of Electrical and Computer Engineering, Yokohama National University, Yokohama, Japan, where he is currently an Associate Professor. From 2003 to 2004, he was a Visiting Scientist at the Division of Engineering and Applied Sciences, Harvard University, Cambridge, MA.

Dr. Ochiai was a recipient of a Student Paper Award from the Telecommunications Advancement Foundation in 1999 and the Ericsson Young Scientist Award in 2000.

Ryuji Kohno (S'81–M'84) received the Ph.D. degree from the University of Tokyo, Tokyo, Japan, in 1984.

He is currently a Professor of Physics, Electrical and Computer Engineering, Yokohama National University, Yokohama, Japan. He was a Director of the Advanced Telecommunications Laboratory, SONY CSL, during 1998–2002, and is currently a Director of Ultra-Wideband (UWB) Technology Institute, National Institute of Information and Communications Technology (NICT).

Prof. Kohno was awarded the Institute of Electrical, Information, and Communication Engineers (IEICE) Greatest Contribution Award and the NTT DoCoMo Mobile Science Award in 1999 and 2002, respectively. He was elected as a member of the Board of Governors of the IEEE Information Theory (IT) Society in 2000 and 2003. He was an Editor of the IEEE TRANSACTIONS ON INFORMATION THEORY, the IEEE TRANSACTIONS ON COMMUNICATIONS, and the IEEE TRANSACTIONS ON INTELLIGENT TRANSPORTATION SYSTEMS (ITS). He is a Fellow of IEICE, Vice President of Engineering Sciences Society of IEICE, and has been the Chairman of the IEICE Technical Committee on Spread-Spectrum Technology, ITS, and Software Defined Radio (SDR). He has organized many international conferences and was Chair-In Honor of the 2002 and 2003 International Conference of SDR (SDR'02 and SDR'03), a TPC Co-Chair of the 2003 International Workshop on UWB Systems (IWUWBS'03), and a General Co-Chair of the 2003 IEEE International Symposium on IT (ISIT'03) and the joint UWBST and IWUWB'04.

PAPER Special Section on Information Theory and Its Applications

Space-Time-Frequency Turbo Code over Time-Varying and Frequency-Selective Fading Channel

Kouji ISHII[†*a)], *Member and* Ryuji KOHNO[†], *Fellow*

SUMMARY In this paper, we propose and investigate space-time-frequency turbo coded OFDM transmissions through time-varying and frequency-selective fading channel. The proposed turbo code is a serial concatenated convolutional code which consists of space-frequency and time-frequency domain codes. The aim of the proposed turbo code is to obtain both diversity and coding gains over space-time-frequency domain. Using computer simulations and EXtrinsic Information Transfer (EXIT) charts, we investigate the optimum structure of inner and outer codes. Simulations demonstrate that the proposed system leads to significantly enhanced performance. Moreover, we analyze the computational complexity.

key words: turbo code, space-time-frequency code, iterative decoding, EXIT chart, OFDM, MIMO

1. Introduction

Recently, there are a lot of demands for high-speed wireless data transmissions over 100 Mbps. In order to achieve this, it is very important to improve frequency efficiency. One of the techniques which can improve bandwidth efficiency is multiple input multiple output (MIMO) channel communication [1]–[10]. In MIMO communications, the transmitter and receiver have multiple antennas. There are two techniques for MIMO communications. One is spatial division multiplexing (SDM) [1]–[4]. SDM involves transmitting independent streams of data across multiple antennas to maximize throughput. Another is a space-time coding (ST coding) [5]–[8]. ST coding appropriately maps input symbol streams across space and time in order to obtain transmit diversity and coding gain at the transmitter. On the other hand, as a high-speed data transmission technique and a countermeasure technique against inter-symbol interference (ISI), orthogonal frequency division multiplexing (OFDM) has received a lot of attention. Due to cyclic prefix (CP) insertion, the channel of OFDM transmission can be considered as ISI-free (if the length of channel delay is less than the length of CP). Since an ST coding technique is weak against ISI, there is a lot of attention to a combination between ST coding techniques and OFDM transmission. However, ST coding is designed for narrowband channel where spatial diversity is only available (in the case of frequency-flat and slow fading). For broadband channels (i.e., channels with delay spread), space-frequency (SF) coding has been designed in order to obtain both spatial and frequency diversity [8], [9].

In this paper, we pay attention to space-time-frequency (STF) coded OFDM transmissions over frequency selective Rayleigh fading channels. There has been a lot of investigation into the design criteria of ST, SF and STF codes [5]–[10]. These criteria, however, are not designed taking channel coding into account. In order to achieve high-reliability communications, it is necessary to optimize the system considering both an error correcting and an STF (ST, SF) coding technique. In this paper, we propose and investigate the structure of concatenation between SF and time-frequency (TF) domain channel codes. Due to concatenating other domain code, we aim to obtain both diversity and coding gain in space, time and frequency domain. The proposed encoder structure consists of a channel encoder in TF domain and an SF code with an interleaver between each encoder. We consider the channel encoder as the outer encoder and the SF encoder as the inner encoder. Then, the proposed encoder structure can be considered as a serial concatenation code between TF and SF encoders, while, the decoder can operate iteratively in space, time and frequency domains. Therefore, the proposed system can achieve the both diversity and coding gain over space, time and frequency. The key point of the proposed code is the concatenation between different domain codes (an SF code and a TF code). In the case of decoding process of the SF code, the decoder can utilize the TF domain information as the *a priori* information. On the other hand, in the case of decoding process of the TF code, the decoder can utilize the SF domain information as the input information. This is one cycle of decoding process. The decoder can decode iteratively with this cycle. Therefore, the proposed concatenated code can achieve the both diversity and coding gain of all domain, totally.

In order to analyze the iterative processing (e.g., turbo equalizer, iterative decoding), EXIT chart analysis has been proposed [15]–[17]. Using EXIT chart analysis, we investigate the optimum structure of inner and outer codes. The major contributions of this paper are the following.

- For multiantenna OFDM systems through time-varying and frequency-selective Rayleigh fading channels, we can effectively achieve high coding and diversity gain over space, time and frequency.
- We analyze the optimum structure of each element code for the proposed STF turbo code using computer

Manuscript received January 24, 2005.
Manuscript revised April 27, 2005.
Final manuscript received June 9, 2005.

[†]The authors are with the Division of Electrical and Computer Engineering, Faculty of Engineering, Yokohama National University, Yokohama-shi, 240-8501 Japan.
[*]Presently, with Kagawa University.
a) E-mail: kishii@eng.kagawa-u.ac.jp

DOI: 10.1093/ietfec/e88–a.10.2885

simulations and EXIT charts.
- We analyze the computational complexity of the proposed system.

This paper is organized as follows. In Sect. 2, we describe the STF coded OFDM transmission system through time-varying and frequency-selective channels. In Sect. 3, we propose a concatenated encoding scheme between SF and TF codes and its iterative decoding scheme. In Sect. 4, we evaluate the proposed system by computer simulations. In Sect. 5, we analyze the optimum inner/outer code for STF turbo code using EXIT chart. In Sect. 6, we analyze the computational complexity of the proposed decoding scheme. In Sect. 7, we conclude this paper.

2. STF Coded OFDM Transmission through Time-Varying and Frequency-Selective Fading Channels

In this section, we describe the system model. Figure 1 depicts a multi-antenna OFDM transmission model with N_t transmit antennas and N_r receive antennas. One OFDM frame consists of N_c subcarriers and N_s symbols. We define the channel response between the μth transmit antenna and the νth receive antenna at time n as $\mathbf{h}^n_{\mu\nu}$. $\mathbf{h}^n_{\mu\nu}$ is a frequency-selective and time varying channel response described by the discrete-time baseband equivalent impulse response vector $[h^n_{\mu\nu}(0), \cdots, h^n_{\mu\nu}(L)]^T \in \mathbf{C}^{(L+1)\times 1}$, where L stands for the channel order. $x^\mu_n(p)$ shows the data symbol transmitted on the pth ($p \in [1, \cdots, N_c]$) subcarrier from the μth ($\mu \in [1, \cdots, N_t]$) transmit antenna during the nth ($n \in [1, \cdots, N_s]$) OFDM symbol interval. The transmit symbols are inverse-fast-Fourier-transformed (IFFT), CP inserted and transmitted with each transmit antenna. The length of CP is defined as L. At the receiver side, each antenna receives faded signals which are transmitted from multi-antenna. We assume that carrier synchronization and channel estimation are ideal. The receiver removes CP from the received signals and does a fast-Fourier-transform (FFT). As the results of those processes, we get $y^\nu_n(p)$ representing the signal of the νth receive antenna, nth symbol and pth subcarrier. Therefore, $y^\nu_n(p)$ can be expressed as

$$y^\nu_n(p) = \sum_{\mu=1}^{N_t} H^n_{\mu\nu}(p)x^\mu_n(p) + \omega^\nu_n(p) \quad (1)$$
$$\nu = 1, \cdots N_r$$
$$n = 1, \cdots N_s$$

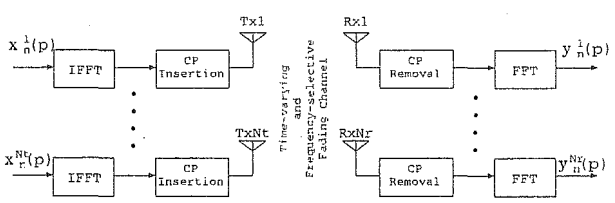

Fig. 1 System model of multi-antenna OFDM transmission between the transmit symbols x and the receive symbols y.

$$p = 1, \cdots N_c$$

where $H^n_{\mu\nu}(p)$ is the channel gain of pth subcarrier nth symbol from the μth transmit antenna to the νth receive antenna, and $\omega^\nu_n(p)$ is the complex additive white Gaussian noise (AWGN) of νth receive antenna, nth symbol and pth subcarrier with zero mean and variance N_0. $H^n_{\mu\nu}(p)$ is defined as

$$H^n_{\mu\nu}(p) = \sum_{l=0}^{L} h^n_{\mu\nu}(l)e^{-j(2\pi/N_c)lp}. \quad (2)$$

Equation (1) can be rewritten in a 3-D matrix as follows;

$$\mathbf{Y}(p) = \mathbf{H}(p)\mathbf{X}(p) + \mathbf{W}(p). \quad (3)$$

Equation (3) shows the MIMO OFDM transmission system with N_t transmit antenna, N_r receive antenna, N_c subcarriers and N_s symbols. Equation (3) can be calculated as follows:

$$\begin{bmatrix} y^1_1(p) \\ y^2_1(p) \\ \vdots \\ y^{Nr}_1(p) \end{bmatrix} = \mathbf{H}(p,1) \begin{bmatrix} x^1_1(p) \\ x^2_1(p) \\ \vdots \\ x^{Nt}_1(p) \end{bmatrix}$$
$$\vdots$$
$$\begin{bmatrix} y^1_{Ns}(p) \\ y^2_{Ns}(p) \\ \vdots \\ y^{Nr}_{Ns}(p) \end{bmatrix} = \mathbf{H}(p,Ns) \begin{bmatrix} x^1_{Ns}(p) \\ x^2_{Ns}(p) \\ \vdots \\ x^{Nt}_{Ns}(p) \end{bmatrix} \quad (4)$$

where

$$\mathbf{H}(p,n) = \begin{bmatrix} h^n_{1,1} & \cdots & h^n_{1,Nt} \\ \vdots & \ddots & \\ h^n_{Nr,1} & \cdots & h^n_{Nr,Nt} \end{bmatrix}. \quad (5)$$

The received signal matrix $\mathbf{Y}$ over STF domains is given by

$$\mathbf{Y} = [\mathbf{Y}(1), \cdots, \mathbf{Y}(N_c)] \in \mathbf{C}^{N_r \times N_s N_c} \quad (6)$$

where

$$\mathbf{Y}(p) = \begin{bmatrix} y^1_1(p) & \cdots & y^1_{N_s}(p) \\ \vdots & \ddots & \vdots \\ y^{N_r}_1(p) & \cdots & y^{N_r}_{N_s}(p) \end{bmatrix} \in \mathbf{C}^{N_r \times N_s}. \quad (7)$$

The transmit symbol matrix $\mathbf{X}$, which is encoded over STF domains is given by

$$\mathbf{X} = [\mathbf{X}(1), \cdots, \mathbf{X}(N_c)] \in \mathbf{C}^{N_t \times N_s N_c} \quad (8)$$

where

$$\mathbf{X}(p) = \begin{bmatrix} x^1_1(p) & \cdots & x^1_{N_s}(p) \\ \vdots & \ddots & \vdots \\ x^{N_t}_1(p) & \cdots & x^{N_t}_{N_s}(p) \end{bmatrix} \in \mathbf{C}^{N_t \times N_s}. \quad (9)$$

$\mathbf{H}(p)$ shows the frequency-selective and time variant multi-carrier MIMO channel matrix ($\mathbf{H}(p) \in \mathbf{C}^{Nr \times N_t \times N_s}$) with (ν, μ, n)th entry $[\mathbf{H}(p)]_{\nu\mu n} = H^n_{\mu\nu}(p)$. In this paper, we propose and investigate the way to obtain the encoded signal $\mathbf{X}$ and decode the receive signal $\mathbf{Y}$.

3. Concatenated Scheme with Time-Frequency and Space-Frequency Domain Codes

In this section, we describe an encoding scheme exploiting STF domains and its decoding scheme in order to obtain the maximum diversity and coding gain.

3.1 Concatenated Encoding Scheme over STF Domains

In this subsection, we describe the structure of the proposed concatenated code consisting of a TF domain error correcting code and an SF code. We recall that the channel is a time-varying and frequency-selective Rayleigh fading channel with channel order of length L. We consider the channel as an ISI-free channel, because the length of CP is L. Therefore in this paper we do not take multipath diversity techniques [8] into account.

Figure 2 shows the block diagram of the proposed serial concatenated encoder. First, the binary information data $\mathbf{b}_i$ are encoded to the binary data $\mathbf{b}_c$ by a channel (outer) encoder Θ over the TF domain, as follows:

$$\Theta : \mathbf{b}_i \rightarrow \mathbf{b}_c \tag{10}$$

where $\mathbf{b}_i \in \mathbf{C}^k, \mathbf{b}_c \in \mathbf{C}^n$. Therefore, the rate r_c of the outer code in TF domains is $R_{ch} = \frac{k}{n}$. Second, the coded data is interleaved as follows:

$$\pi : \mathbf{b}_c \rightarrow \mathbf{b'}_c \tag{11}$$

where π is defined as the interleaver function and $\mathbf{b'}_c \in \mathbf{C}^n$. Third, the interleaved data $\mathbf{b'}_c$ is mapped to constellation point $\mathbf{S}$, and SF encoded as follows:

$$\Phi : \mathbf{b'}_c \rightarrow \mathbf{S} \tag{12}$$

$$\Psi : S \rightarrow \mathbf{X} \tag{13}$$

where $\mathbf{S}$ is the modulated symbol, $\mathbf{X}$ is the transmit symbol set, Φ is the mapping function from binary to symbol and Ψ is SF mapping function. $\mathbf{S}$ is chosen from $\mathcal{A}_X$ (in the case of QPSK transmissions, $\mathcal{A}_X$ belongs to [0,1,2,3]). The $[\mathbf{X}]_{\mu np}$ which represents μth transmit antenna, nth symbol interval, pth subcarrier transmit signal is also chosen from $\mathcal{A}_X$. $|\mathcal{A}_X|$ is the cardinality of $\mathcal{A}_X$. The transmit rate is therefore $R_T = R_{ch} \log_2 |\mathcal{A}_X|$ bit/sec/Hz in the case that we ignore the decrease in the transmission rate due to inserting the pilot signal and CP. Finally, the encoded signals $\mathbf{X}$ are OFDM-modulated (derived by IFFT), CP inserted and transmitted using multiple transmit antennas.

For broadband channels, SF code is designed in order to obtain both spatial and frequency diversity [9]. Then, in this paper, we use not ST but SF code as an inner code.

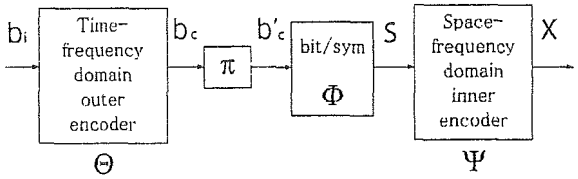

Fig. 2 Block diagram of concatenated encoder between a time-frequency and a space-frequency domain codes.

3.2 Iterative Decoding Scheme

In this subsection, we describe the iterative decoding scheme which can obtain maximum coding and diversity gains over the STF domains. Figure 3 shows the proposed iterative decoder structure. The SISO MAP decoder in Fig. 3 stands for Soft-Input Soft-Output Maximum *a posteriori probability* decoder. The SISO MAP decoder consists of 2-input and 2-output components. The SISO MAP decoder requires both the *a priori* information and the *logarithmic likelihood ratios* (LLRs). The LLRs are computed from received signals. The SISO MAP decoder computes the two *extrinsic information* sequences that are for the information and code symbols. For the sake of simplicity, we omit the FFT branch and the cyclic prefix remover in Fig. 3. Figure 3 shows the latter part of Fig. 1. Recall that the input of the iterative decoder is $\mathbf{Y}$. Therefore, the iterative decoder estimates the information data from the received signal matrix $\mathbf{Y}$.

We give an overview of the decoding process as follows. First, the symbol-symbol MAP decoder for the inner code (SF code) computes the *extrinsic information* using the LLRs and the *a priori probability*. In the case of the first iteration, the *a priori probability* is $1/|\mathcal{A}_x|$. Second, the results of the MAP decoder of the SF code are transformed from symbol to binary domain probabilities. Third, the binary domain results are deinterleaved. Fourth, the MAP decoder for the outer code (TF domain error correcting code) decodes with the deinterleaved binary probabilities. Fifth, the results of outer MAP decoder are interleaved and transformed to symbol domain probabilities. Sixth, we consider the symbol domain probabilities as the *a priori probability* for the inner MAP decode. This cycle is one decoding process. We decode iteratively with this cycle. We now describe each part of the decoding technique in detail. First, we consider the SISO MAP decoder for the SF (inner) code. Recall that the kind of SISO MAP decoder for the SF code is a symbol-symbol MAP decoder. Therefore, the SISO MAP decoder calculates the *a posterior probability* (APP) from

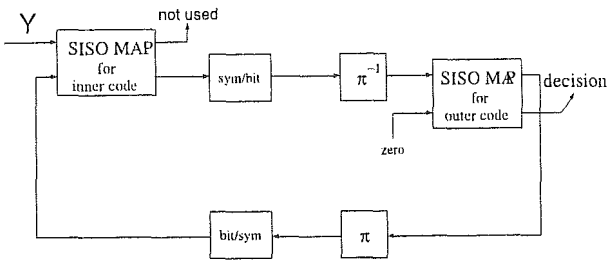

Fig. 3 Iterative decoder structure for space-time-frequency domain serial concatenated coded OFDM.